SOURCE DATA   TRANSPARENT PROCESS   OPEN ACCESS

Octarepeat region flexibility impacts prion function, endoproteolysis and disease manifestation

Agnes Lau[1,2], Alex McDonald[3], Nathalie Daude[1], Charles E Mays[1], Eric D Walter[3], Robin Aglietti[3], Robert CC Mercer[1], Serene Wohlgemuth[1], Jacques van der Merwe[1], Jing Yang[1], Hristina Gapeshina[1], Chae Kim[4], Jennifer Grams[1], Beipei Shi[1], Holger Wille[1,5], Aru Balachandran[6], Gerold Schmitt-Ulms[7], Jiri G Safar[4], Glenn L Millhauser[3] & David Westaway[1,2,5,*]

Abstract

The cellular prion protein (PrP^C) comprises a natively unstructured N-terminal domain, including a metal-binding octarepeat region (OR) and a linker, followed by a C-terminal domain that misfolds to form PrP^{Sc} in Creutzfeldt-Jakob disease. PrP^C β-endoproteolysis to the C2 fragment allows PrP^{Sc} formation, while α-endoproteolysis blocks production. To examine the OR, we used structure-directed design to make novel alleles, 'S1' and 'S3', locking this region in extended or compact conformations, respectively. S1 and S3 PrP resembled WT PrP in supporting peripheral nerve myelination. Prion-infected S1 and S3 transgenic mice both accumulated similar low levels of PrP^{Sc} and infectious prion particles, but differed in their clinical presentation. Unexpectedly, S3 PrP overproduced C2 fragment in the brain by a mechanism distinct from metal-catalysed hydrolysis reported previously. OR flexibility is concluded to impact diverse biological endpoints; it is a salient variable in infectious disease paradigms and modulates how the levels of PrP^{Sc} and infectivity can either uncouple or engage to drive the onset of clinical disease.

Introduction

Prion diseases such as Creutzfeldt-Jakob disease (CJD) and bovine spongiform encephalopathy (BSE) are transmissible neurodegenerative disorders. The cellular form of the prion protein (PrP^C), encoded by the *Prnp* gene, is displayed on the cell surface by a glycophosphatidylinositol (GPI) anchor and serves a precursor role, undergoing a change from a mainly alpha-helical structure to the beta-rich conformation of PrP^{Sc} during disease. Its function is debated such that it could be involved in neuroprotection (Kuwahara *et al*, 1999; Weise *et al*, 2004; Watt *et al*, 2005; Rangel *et al*, 2007), copper homeostasis (Pauly & Harris, 1998; Herms *et al*, 1999; Millhauser, 2004, 2007), signal transduction (Mouillet-Richard *et al*, 2000; Spielhaupter & Schatzl, 2001; Chiarini *et al*, 2002) or peripheral myelin maintenance (Nishida *et al*, 1999; Bremer *et al*, 2010). In structural terms, PrP^C is composed of a flexible N-terminal region (including a charged patch), two hexarepeats, five tandem repeats of eight amino acids forming an octarepeat region (OR), a hydrophobic linker region sometimes referred to as the 'HD' (hydrophobic domain) and a C-terminal globular domain (Fig 1A).

A number of similarities have emerged between prion diseases and Alzheimer's disease (AD), two having particular relevance here. The first concerns the crucial role of endoproteolytic events. One important misfolded protein species in AD is the amyloid beta peptide, Aβ, this being liberated by the concerted actions of the endoproteases called β- and γ-secretase on the beta amyloid precursor protein, APP. Conversely, α-secretase processing of APP by a disintegrin and metalloproteases (ADAM) generates a benign peptide called P3 and prevents amyloid formation. Notably, PrP^C is subject to analogous endoproteolysis events (Fig 1A); α-cleavage of PrP^C occurs adjacent to the linker region at residue 110 to generate a fragment called C1 and is also attributed to the action of an ADAM protease (Chen *et al*, 1995; Jimenez-Huete *et al*, 1998; Vincent *et al*, 2000, 2001; Laffont-Proust *et al*, 2005; Walmsley *et al*, 2009). Furthermore, α-cleavage of PrP^C serves a benign role insofar as formation of C1 precludes the formation of PrP^{Sc} upon exposure to infectious prion inocula as the protease-resistant core of PrP^{Sc} called PrP27-30 is longer, starting in

1   Centre for Prions and Protein Folding Diseases, University of Alberta, Edmonton, AB, Canada
2   Department of Medicine, University of Alberta, Edmonton, AB, Canada
3   Department of Chemistry and Biochemistry, University of California Santa Cruz, Santa Cruz, CA, USA
4   National Prion Disease Surveillance Center, Departments of Pathology and Neurology, School of Medicine, Case Western Reserve University, Cleveland, OH, USA
5   Department of Biochemistry, University of Alberta, Edmonton, AB, Canada
6   CFIA Lab, Nepean, ON, Canada
7   Tanz Centre for Research in Neurodegenerative Diseases, Department of Laboratory Medicine and Pathobiology, University of Toronto, Toronto, ON, Canada
    *Corresponding author. Tel: +1 780 492 9024; Fax: +1 780 492 9352; E-mail: david.westaway@ualberta.ca
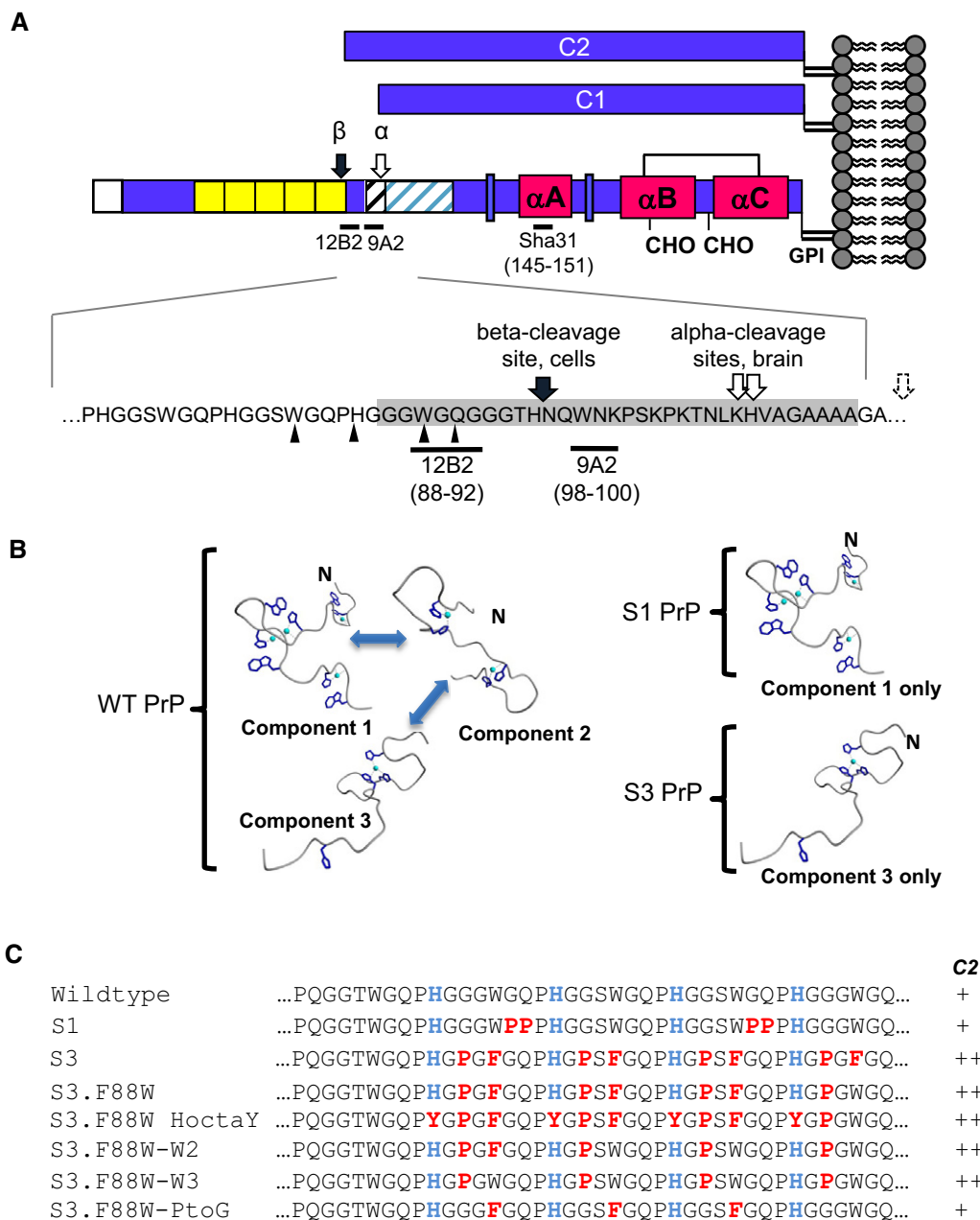
Figure 1. Copper-binding conformations and PrP octarepeat sequence mutations.

A   The structure of full-length PrP and derivative C1 and C2 fragments with an enlarged view of the cleavage sites is shown. The C2 (β) site was mapped in HpL3-4 cells by (Mange et al, 2004). Ragged C1 (α) cleavage sites in brain are shown (Chen et al, 1995), and a dotted arrow indicates that additional sites have been mapped rightward of this position in vitro (McDonald et al, 2014). Ragged N-terminal cleavage sites of PrP27-30 from prion-infected mouse brain are indicated by small arrows (Howells et al, 2008). The positions of antibody epitopes are also shown (residues in brackets). Grey shading reflects the minimum length for a C2 fragment defined operationally by reactivity with 12B2 antibody.

B   S1 and S3 alleles, by virtue of limited geometries (modified from Chattopadhyay et al, 2005), may have access to distinct subsets of the full range of biological activities of WT PrP, which has access to interchangeable component 1, 2 and 3 geometries.

C   Sequences of synthetic PrP alleles differing in the octarepeat region of mouse PrP. Conserved histidines in octarepeats 2–5 are coloured blue and missense mutations are shown in red. Overproduction of C2 fragment is indicated by ++ signs to the right of the panel.

the vicinity of residue 90 (Prusiner et al, 1984; Oesch et al, 1985). Indeed, recent studies have shown that expression of C1 PrP may be protective during disease (Lewis et al, 2009; Westergard et al, 2011). Conversely, β-processing to make C2 PrP is thought to be conducive to prion replication and while in vivo cleavage of APP by β-secretase, BACE1, is well understood, this is not the case for C2 PrP, where facilitated cleavage has only been produced in vitro (McMahon et al, 2001; Watt et al, 2005).

The second similarity between prion disease and AD concerns the assignment of crucial pathogenic pathways. While PrP and Aβ are the aetiological causative agents defined by many transmission studies and genetics, respectively, the exact physical forms of the agents that cause toxicity at disease end-stage—perhaps oligomeric assemblies for Aβ and perhaps a 'lethal' PrP form denoted PrP^L—have proven difficult to study (Legname et al, 2004; Sandberg et al, 2011; Aguzzi & Falsig, 2012; Benilova et al, 2012). In the case of prions, instances of apparent uncoupling between the accumulation of protease-resistant PrP and clinical signs of disease caused confusion in the field and were once used to argue against the validity of the prion hypothesis (Lasmezas et al, 1997).

The studies presented here focus upon PrP N-terminal sequences. Though not obligatory for laboratory infection of rodents (Fischer et al, 1996; Flechsig et al, 2000), extra copies of the octarepeats to make an expanded OR are associated with familial prion diseases with heterogeneous clinical presentations, being variously classified as genetic CJD, Gerstmann–Sträussler–Scheinker syndrome or psychiatric disorders (Goldfarb et al, 1991; Laplanche et al, 1999; Moore et al, 2001; Mead et al, 2006). N-terminal sequences are thought to bind a number of partners (Beland & Roucou, 2012), with binding of Cu(II) and Zn(II) ions by the OR being an area of active interest (reviewed in Millhauser, 2007). Based on the concept that the N-terminal region of metal-free PrP^C (apo-PrP^C) is natively unstructured but that different stoichiometries of metal binding can impart different structures upon the OR (called 'component 1', 'component 2' and 'component 3' (Chattopadhyay et al, 2005); Fig 1B), we used structure-guided design to create new PrP alleles (Fig 1C). While conformation components 1, 2 and 3 may interchange depending upon local physiological conditions, we were interested in the concept that they have different functions and sought to restrict inter-conversion to study their biological properties individually. One new PrP allele called 'S1' locks the OR in an extended conformation (component 1 metal-binding geometry), and this conformation is conducive to binding up to 4 copper ions per OR. Another allele called 'S3' locks PrP in a compact conformation that can bind only one copper ion per OR, corresponding to component 3 metal-binding geometry (the intermediate conformation component 2 was not modelled in our studies). The S1 and S3 PrP alleles were expressed in cells and transgenic mice and revealed a number of unexpected interrelationships between OR flexibility, physiological function, pathogenesis of infectious disease and β-cleavage.

Results

Increased C2 fragment levels are associated with S3 PrP, not S1 PrP

Using a series of synthetic peptides and electron paramagnetic resonance (EPR) analysis of metal protein complexes, we identified residue substitutions in ORs 2–5 that constrained PrP to favour component 1 or 3 binding geometry (Supplementary Fig S1) (Chattopadhyay et al, 2005). We then derived the corresponding mutant alleles of the Prnp gene S1 PrP and S3 PrP (as well as a WT control construct equipped with the same 5′ UTR leader sequences) that could encode the conformationally constrained proteins (Fig 1B

and C). To confirm expression, the plasmids were transiently transfected into RK13 cells and lysates analysed for PrP^C by Western blot with the antibody Sha31 (Feraudet et al, 2005) after PNGaseF treatment to remove glycans (Fig 2A). The S1 and S3 alleles were glycosylated in a similar manner to WT PrP and showed similar localization within permeabilized RK13 cells (Supplementary Fig S2A and B). Deglycosylated samples showed full-length (FL) PrP and C1 PrP, but cells expressing S3 PrP also had increased levels of the C2 fragment (Fig 2A). To confirm these data, PrP antibodies 9A2 and 12B2 were used (Fig 2A), which do not recognize the C1 fragment due to the location of their epitopes (Fig 1A). No signal was observed for S3 PrP using the 12B2 antibody, but a tryptophan residue of this antibody's epitope is altered in S3 PrP. Since this amino acid change was close to the 'beta' cleavage site observed in infected tissue (Chen et al, 1995; Mange et al, 2004), we reverted a phenylalanine in S3 to the WT residue at this position, tryptophan (S3.F88W). Using Sha31 and 9A2 antibodies, we observed that the C2 fragment remained prominent in RK13 cells expressing the F88W plasmid. When the 12B2 antibody was applied, signal for FL and C2 PrP returned (Fig 2A), indicating that a cleavage site to generate C2 PrP from the S3 allele is positioned N-terminal to residue 88 (Fig 1A).

Based on these results, we generated stable RK13 clones expressing WT PrP (WT-10), S1 PrP (S1–29), S3 PrP (S3–27) and S3.F88W PrP (F88W-5). Cell surface proteins were biotin-labelled using a membrane-impermeable reagent and trypsin-digested following specific chase times (Supplementary Fig S2C). The mutant S1 and S3 full-length PrP, as well as the C2 fragment, was found to be accessible on the surface of cells, and the mutants were internalized with similar kinetics to a WT PrP control.

Effects of histidine substitutions and cell type on C2 cleavage of S3 PrP

The levels of endogenous copper in our cell media were determined to be between 0.46 μM and 1.4 μM (average = 0.85 μM ± 0.14 SEM, $n = 5$), but a series of experiments modulating these baseline values by adding chelators or metals or by altering cell plating density failed to alter C2 formation by the S3 or WT PrP alleles (Supplementary Figs S3, S4 and S5). As PrP^C's component 3 geometry binds copper using OR histidines (Stöckel et al, 1998; Viles et al, 1999; Chattopadhyay et al, 2005), we assessed the effect of mutating these residues to tyrosine ('S3.F88W HoctaY' allele). As presented in Fig 2B, the C2 fragment was observed in cells expressing the S3.F88W HoctaY mutant, indicating that the increased levels of C2 fragment associated with S3 and S3.F88W PrP were prompted by effects of the residue substitutions and unrelated to metal occupancy in vivo. This conclusion was emphasized by a further mutant that also produced abundant C2, S3.HoctaY.H95A, where His 95 of the non-OR 'copper site 5′ (Jackson et al, 2001) was replaced by an alanine residue to result in a net perturbation of all major copper-binding sites in PrP^C's N-terminus.

To define the residues responsible for altered cleavage of PrP, we reverted substitutions within S3 PrP back to their WT status (Fig 1C) and transfected these plasmids into RK13 cells. The C2 fragment was present in lysates from cells expressing S3.F88W-W2 (substitutions to proline and phenylalanine in octarepeat 2 and prolines in octarepeats 3–5) and S3.F88W-W3 (substitutions to
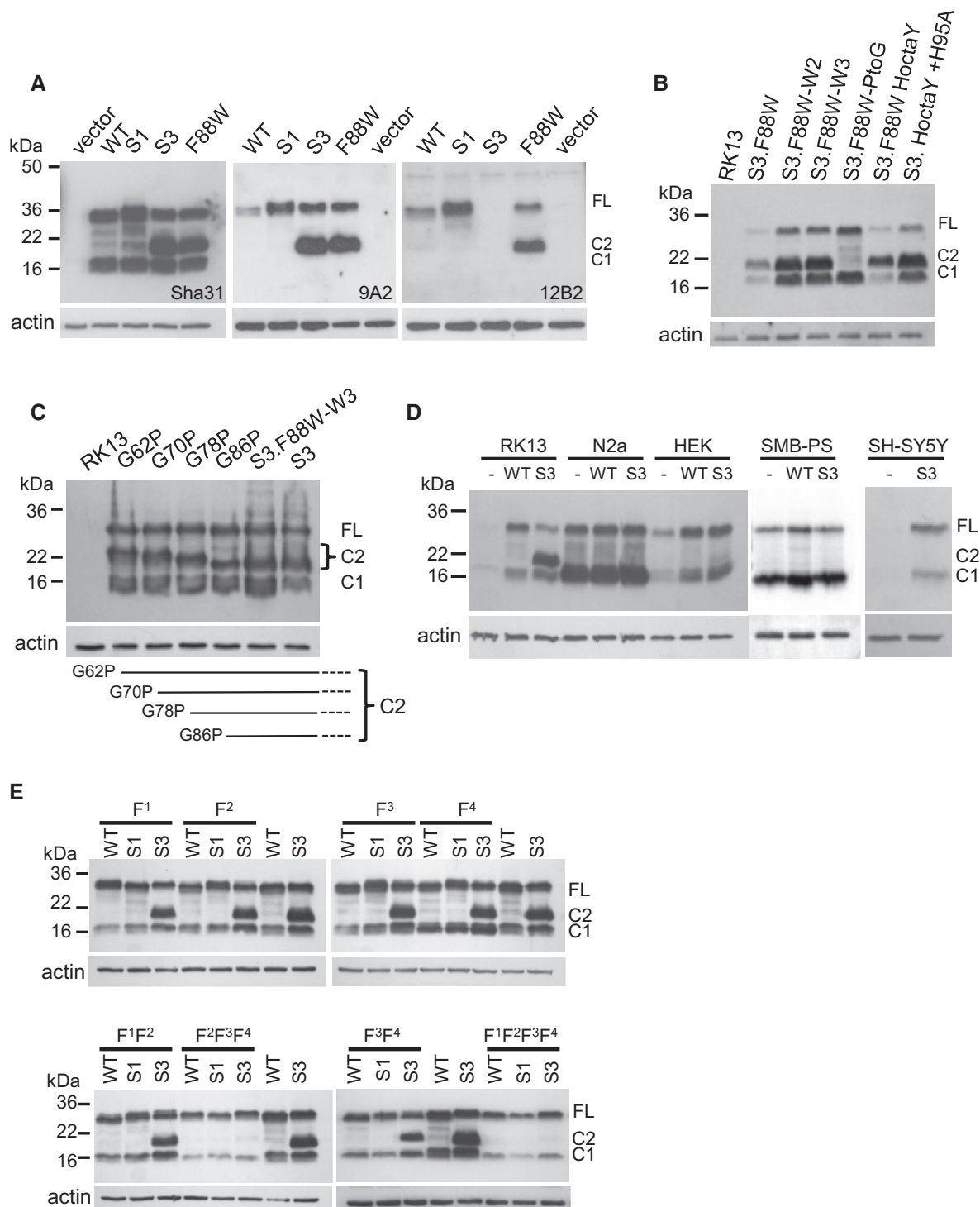
Figure 2. Western blot analysis of lysates from cells transiently transfected with plasmids encoding PrP mutants.

A   Lysates from RK13 cells transfected with WT, S1, S3 and S3.F88W PrP were probed with antibody Sha31, 9A2 and 12B2 after digestion with PNGaseF.

B, C   Additional PrP mutants were examined by Western blot with Sha31 after PNGaseF digestion of RK13 cell lysates. A schematic of the different lengths of C2 caused by single mutations in the OR is shown in the lower portion of (C).

D   Lysates of N2a, HEK, SMB-PS and SH-SY5Y cells not transfected (−) and transiently transfected with WT PrP or S3 PrP plasmids were digested with PNGaseF and analysed by Western blot using Sha31.

E   Analysis of lysates from RK13 cells transfected with plasmids incorporating Phe substitutions into the hydrophobic domain of WT PrP, S1 PrP and S3 PrP. Lysates were PNGaseF-digested before Western blot using the Sha31 antibody. F[1]: A114F, F[2]: G118F, F[3]: G122F, F[4]: G126F

Source data are available online for this figure.

proline in octarepeats 2–5), but was absent from cells expressing S3.F88W-PtoG, which had substitutions to phenylalanine in octarepeats 2–4 (Fig 2B). This indicated that the PHGGGWGQ-> PHGPGWGQ proline substitutions within S3 PrP determine C2 cleavage. To test this concept further, we mutated individual prolines within octarepeats 2, 3, 4 and 5. Proceeding in reverse order from octarepeat 5 through octarepeat 2 (i.e. proceeding in an N-terminal direction), the size of the C2 fragment increased accordingly and was compatible with one cleavage per PHGPGWGQ-containing octarepeat (Fig 2C).

Endoproteolysis of PrP^C to C2 fragments has previously been suggested to occur through reactive oxygen species (ROS) generated by the binding of copper to the PrP OR (McMahon *et al*, 2001; Pushie & Vogel, 2008, 2009), where the free radicals react with a peptidyl bond and cause cleavage. However, the C2 fragment was produced in cells expressing S3.F88W HoctaY, which cannot bind copper via the OR. Moreover, the mechanism proposed from previous *in vitro* studies only requires PrP, a ROS-generating system, and copper for an autocatalytic reaction; however, when the S3 PrP plasmid was introduced into four cell lines other than RK13, the C2 fragment was not detected (Fig 2D). This indicates that other factors may affect cleavage, such as a protease present in RK13 cells yet absent from N2a, HEK, SH-SY5Y and SMB-PS cells.

Hydrophobic domain substitutions impact β-cleavage of S3 PrP

Due to the possibility of N-terminal/C-terminal interactions occurring in *cis* (Thakur *et al*, 2011; Sonati *et al*, 2013; Spevacek *et al*, 2013), we investigated whether bulky side-chain substitutions that might interfere with the flexibility of the intervening linker region could affect C2 cleavage. As seen in Fig 2E, when residues 114G, 118G, 122G and 126G were mutated to phenylalanine individually or in pairs (F^1F^2; F^3F^4), there was no effect on the cleavage of S3 PrP. However, if compounded into triple or quadruple mutations ($F^2F^3F^4$ and $F^1F^2F^3F^4$), C2 production was attenuated. There was no visible influence of the phenylalanine residue substitutions on PrP with WT or S1 versions of the OR, and cleavage to the C1 fragment was maintained in cells expressing all mutation variants (Fig 2E).

### Effects of S1 and S3 alleles in uninfected animals

Next, Tg mice were created using a 'half-genomic' construct expression vector derived from the mouse *Prnp* locus (Borchelt *et al*, 1996; Fischer *et al*, 1996). Since the S3.F88W PrP allele was associated with increased levels of the C2 fragment like S3 PrP (Fig 2A), this was used for transgenesis instead of S3 PrP, to allow the 12B2 antibody to be used for protein expression analysis. Following standard pronuclear microinjection procedures, we established 6 new transgenic lines from founder animals. Brain homogenates of adult Tg mice (i.e. TgPrP(WT), TgPrP(S1)-17 and TgPrP(S3.F88W)-35) were analysed for PrP by Western blot using the antibodies Sha31, 12B2 and 9A2 (Fig 3A). High levels of the C2 fragment were observed in TgPrP(S3.F88W)-35 mice. After normalization to full-length brain PrP, densitometric analysis indicated an increment in excess of three-fold (WT C2:C1 0.34:1 ± 0.07 SEM *n* = 7 versus TgS3.F88W 1.14:1 ± 0.06, *P* = 1.46E-06; Fig 3B), which is consistent with densitometric analysis from S3 vs WT PrP-expressing RK13 cells

(Fig 3B right panel). Furthermore, albeit present at lower levels, C2 fragment was detected in non-transgenic mice using the 12B2 antibody, confirming that WT PrP^C is cleaved at a position N-terminal to amino acid 88 to produce the C2 fragment under physiological conditions. We assessed the amount of FL PrP^C and its C1 and C2 fragments in uninfected transgenic mice by Western blot analysis of brain homogenates using six distinct antibodies (Table 1, Supplementary Fig S6). TgPrP(S3.F88W) lines 35 and 14 over-expressed FL PrP approximately 3× WT levels. Two lines of TgPrP(S1) mice had 1.7–1.8× the amount of PrP compared with WT mice, whereas a third line TgPrP(S1)-39 expressed low levels of PrP (0.7×) that were similar to TgPrP(WT) (Supplementary Fig S6; Mays *et al*, 2014). Using synchrotron-based techniques for neuroanatomical mapping of trace metals (Pushie *et al*, 2011), we confirmed altered distribution of Cu and Zn ions in TgPrP(S1) and TgPrP(S3.F88W) mice (M.J. Pushie, A. McDonald, K.H. Nienaber, R. Aglietti, A. Lau, D. Westaway, G.N. George, in preparation).

When different tissues of a TgPrP(S3.F88W)-35 mouse were analysed, the ratios of C2 fragment to C1 or full-length PrP^C differed (Fig 3C). In the spleen, the dominant band was the C1 fragment, but the C2 fragment was strongest in the heart and lung (Fig 3C). Additionally, the size of the C2 fragment in the kidney appeared to be smaller compared to other tissues. When considered alongside our studies for mutant PrP in tissue-culture cells, these data do not provide strong support for the concept that C2 cleavage of S3 PrP *in vivo* derives from a metal-assisted hydrolysis event mediated by the PrP polypeptide chain itself.

Although increased levels of C2 fragments occur in prion disease states (Chen *et al*, 1995; Yadavalli *et al*, 2004; Dron *et al*, 2010) and mice programmed to express a C2 fragment develop a spontaneous disease syndrome (Colby *et al*, 2010), we were unable to detect spontaneous neurological disease in TgPrP(S1) and TgPrP (S3.F88W) mice at nearly 2 years of age, nor the presence of a PK-resistant PrP species by Western blot of brain homogenates from these mice (Supplementary Table S1).

Outside of the CNS, independent lines of PrP knockout mice exhibit a demyelinating polyneuropathy (DMP) (Nishida *et al*, 1999; Bremer *et al*, 2010), which is also present in our colony of Zrch1 *Prnp*$^{0/0}$ mice at ages greater than or equal to 10 months. To assess the abilities of the S1 and S3.F88W alleles to rescue the DMP phenotype, we examined the status of the sciatic nerve in aged S1 and S3. F88W mice versus *Prnp*$^{0/0}$ mice (Fig 4A, Supplementary Fig S7). Here, genetic complementation analysis revealed that three TgPrP (S1) lines and the TgPrP(WT) line rescued the DMP syndrome (Supplementary Fig S7). These animals express both full-length and C1 PrP in sciatic nerves (Fig 4B), as is the case for the CNS (Fig 3A), which is compatible with the contention that α-cleavage may contribute to peripheral nervous system (PNS) maintenance (Bremer *et al*, 2010). Morphometric analysis of sciatic nerves established that mice with DMP syndrome had less than 40% of nerve cross-sectional area occupied by fibres, whereas this figure was above 50% for animals with genetic rescue of the syndrome (Fig 4C, Supplementary Fig S8). With respect to the amount of PrP^C needed to prevent the DMP syndrome, TgPrP(WT) mice exhibit a low level of expression (Table 1 and Mays *et al*, 2014), which is similar to that of *Prnp*$^{0/+}$ mice with only one copy of the *Prnp* gene per diploid genome (these mice do not exhibit DMP (Bremer *et al*, 2010)). Similarly, TgPrP(S1)-39 mice with expression

A

+ PNGaseF

B

Brain   RK13 cells

C

Higher exposure
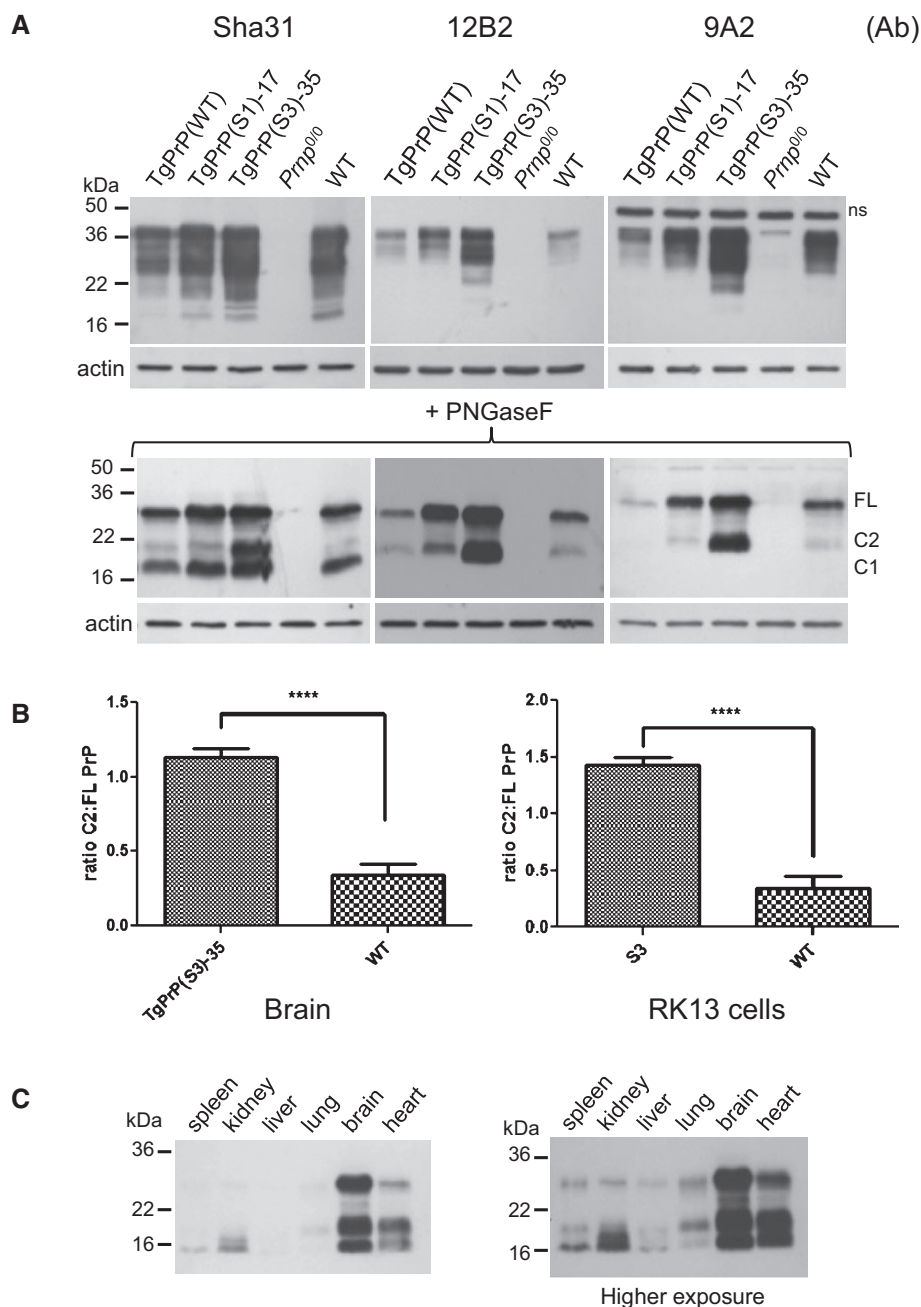
Figure 3. PrP expression in transgenic mice.

A   Brain homogenates of TgPrP(WT), TgPrP(S1)-17 and TgPrP(S3.F88W)-35 mice were analysed by Western blot before and after PNGaseF digestion using the PrP antibodies Sha31, 12B2 and 9A2. Prnp$^{0/0}$, and WT brain homogenates were used as controls.

B   The ratio of C2 to full-length PrP in TgPrP(S3.F88W)-35 and WT mice (left panel, n = 7, P = 1.46E-06) and in RK13 cells expressing WT and S3 PrP (right panel, n = 5, P = 4.01E-05) is shown. Values are presented as mean ± SEM. Unpaired, two-tailed t-test, ****P < 0.0001.

C   Different tissue homogenates from a TgPrP(S3.F88W)-35 mouse were PNGaseF-digested and analysed for PrP using the antibody 1A6. FL, full-length PrP; ns, non-specific signal detected in the immunoblotting procedure.

Source data are available online for this figure.

below endogenous levels (Table 1) do not exhibit the DMP syndrome. Analysis of aged TgPrP(S3.F88W)-35 and TgPrP(S3.F88W)-14 mice (Fig 4A) revealed genetic rescue of the DMP syndrome, albeit with a greater degree of variability. Most TgPrP

(S3.F88W)-35 and TgPrP(S3.F88W)-14 mice had nerve morphology with a uniform distribution of myelinated fibres resembling the WT state. However 20% of TgPrP(S3.F88W) mice had areas of apparently normal fibre morphology lying adjacent to fields of

Table 1. Levels of full-length PrP and PrP fragments in transgenic mice relative to wild-type animals.

Genotype	Full-length (FL) PrP^C determined by Western blot[a]	FL+ C2 PrP^C determined by Western blot[a]	FL+ C2 PrP^C determined by CDI with 12B2 antibody[b]
WT	1.00	1.00	1.00
TgPrP(S1)-17	1.69 ± 0.20	1.49 ± 0.17	1.12 ± 0.14
TgPrP(S1)-19	1.83 ± 0.20	1.58 ± 1.8	1.11 ± 0.14
TgPrP(S1)-39	0.74 ± 0.12	0.57 ± 0.09	0.29 ± 0.04
TgPrP(S3.F88W)-35 male mice	2.93 ± 0.29	4.42 ± 0.67	3.01 ± 0.50
TgPrP(S3.F88W)-14	2.97 ± 0.26	4.56 ± 0.68	4.74 ± 1.32
TgPrP(WT)	0.79 ± 0.15	0.74 ± 0.15	0.43 ± 0.1

[a]Averaged data from adolescent uninfected mice obtained from the use of 12B2, SAF83, 2D6, 9A2, VRQ61 and 1A6 antibodies in Supplementary Fig S6. Apart from the TgPrP(S3.F88W)-35 line, with data just derived from male mice (also applicable to Tables 2 and 3), data were derived from both genders. Ages for the samples range between 37 and 138 days.
[b]The 12B2 epitope lies outside the boundaries of the C1 fragment and hence will detect the sum of full-length PrP^C plus the C2 fragment. These estimates represent PrP^C-containing velocity gradient fractions (fractions 9 and 10) of brain homogenates of uninfected mice at ages 37–80 days; data are derived from 3 mouse brain homogenates per genotype pooled and then gradient-fractionated.

hypermyelinated fibres (Fig 4A), with transmission electron microscopy of samples from the same animals also revealing normally myelinated fibres lying adjacent to hypermyelinated fibres. This variation in gross anatomy was observed alongside larger net variance in percentage of the nerve occupied by fibres for both Tg lines expressing the S3 PrP allele (Fig 4C) and less significant *P*-values versus knockout controls ($P < 0.01$ against $Prnp^{0/0}$ for both Tg lines expressing S3 PrP versus $P < 0.001$ or lower for Tg lines expressing the S1 PrP allele).

Primary passage of the RML prion isolate into TgPrP(S1) and TgPrP(S3.F88W) mice

We next assessed the responses of TgPrP(S1)-17 and TgPrP(S1)-19 mice upon challenge with infectious prions using the RML isolate of mouse-adapted scrapie. As presented in Table 2, mean survival times of TgPrP(S1)-17 mice and TgPrP(S1)-19 mice were either 15 days shorter or indistinguishable from WT mice even though these Tg lines express ~1.7-fold more full-length PrP^C substrate (Table 1; ****$P = 0.0001$ and ns at $P = 0.19$, respectively), with increased expression level being a parameter that normally decreases incubation times (Carlson *et al*, 1994). This indicates that a facet of pathogenesis is attenuated in mice expressing the S1 PrP^C allele. TgPrP(WT) mice (Mays *et al*, 2014) comprised a further control for this experiment; this Tg line had low amounts of PrP and survival times were greater than 400 days, in a similar fashion to hemizygous mice producing ~50% the amount of PrP^C of WT mice (Bueler *et al*, 1994; Fischer *et al*, 1996). More notably, both lines of TgPrP(S3.F88W) mice had incubation times at least 60 days shorter than WT mice (Table 2): 84 and 89 day averages for TgPrP (S3.F88W)-35 and TgPrP(S3.F88W)-14 (****$P = 1.75$E-18 and 2.44E-19, respectively versus WT control).

TgPrP(S1)-17 and TgPrP(S3.F88W)-35 animals were also challenged with prions from cases of natural scrapie and classical BSE. Animals were held for over 400 days without signs of clinical disease (scrapie, range 416–594 dpi; classical BSE, range 445–537 dpi; Supplementary Table S2). These data indicate that typical barriers against the transmission of foreign prions from one species of mammal to another were not circumvented by expression of the S1

and S3.F88W PrP alleles (and in this respect did not differ from the performance of WT PrP (Fraser *et al*, 1992)). Barriers to prion infections can also be caused by PrP coding sequence polymorphism within a species (Carlson *et al*, 1994). These transmission barriers derive from a change in the primary structure of PrP^C substrate and can result in altered selection pressures that will facilitate the emergence of new strains (Collinge & Clarke, 2007). We assessed this possibility for prions deriving from the use of S1 and S3.F88W allelic forms of PrP^C versus WT PrP^C, employing PK digestion to examine changes in glycosylation profile or fragment size of PrP^{Sc}, as well as observing differences in susceptibility to PK digestion after exposure to increasing concentrations of the denaturant guanidine that may indicate a change in structure. However, using the C-terminal antibody Sha31, electrophoretic profiles of PK-digested PrP species from brain homogenates of the transgenic mice were similar to the RML inoculum; this resemblance remained after incubation with the glycosidase PNGaseF, when a single band was present in all three genotypes (Fig 5A and B). Similarly, guanidine denaturation curves of the RML prions propagated in WT mice were similar to those in TgPrP(WT) mice (Fig 5C, Supplementary Fig S9). The guanidine denaturation curves of the RML prions propagated in different Tg lines deriving from the same S3.F88W or S1 PrP constructs (represented by 2 and 3 Tg lines, respectively) were not only similar to each other, but also resembled the denaturation profile of the WT prototypes. These data argue against the emergence of a new prion strain(s) in TgPrP(S1) and TgPrP(S3.F88W) mice infected with the RML prion isolate.

In terms of neuropathology, RML prion-challenged TgPrP(S1) and TgPrP(S3.F88W) exhibited reduced levels of deposition of protease-resistant PrP^{Sc}, reduced gliosis and reduced spongiosis (Fig 6). They did not diverge qualitatively from WT prototypes in that the pattern of PrP^{Sc} deposition did not expand to include novel neuroanatomical structures. Within these immunostaining signals, punctate staining could be seen in some but not all animals, in the corpus callosum, which is analogous to a profile present within WT animals infected with RML prions (Fig 6). Interestingly, the original signature of PrP^{Sc} deposition by the RML agent present in WT animals was retained after three passages through TgPrP(S3.F88W) mice, indicating that expression of the
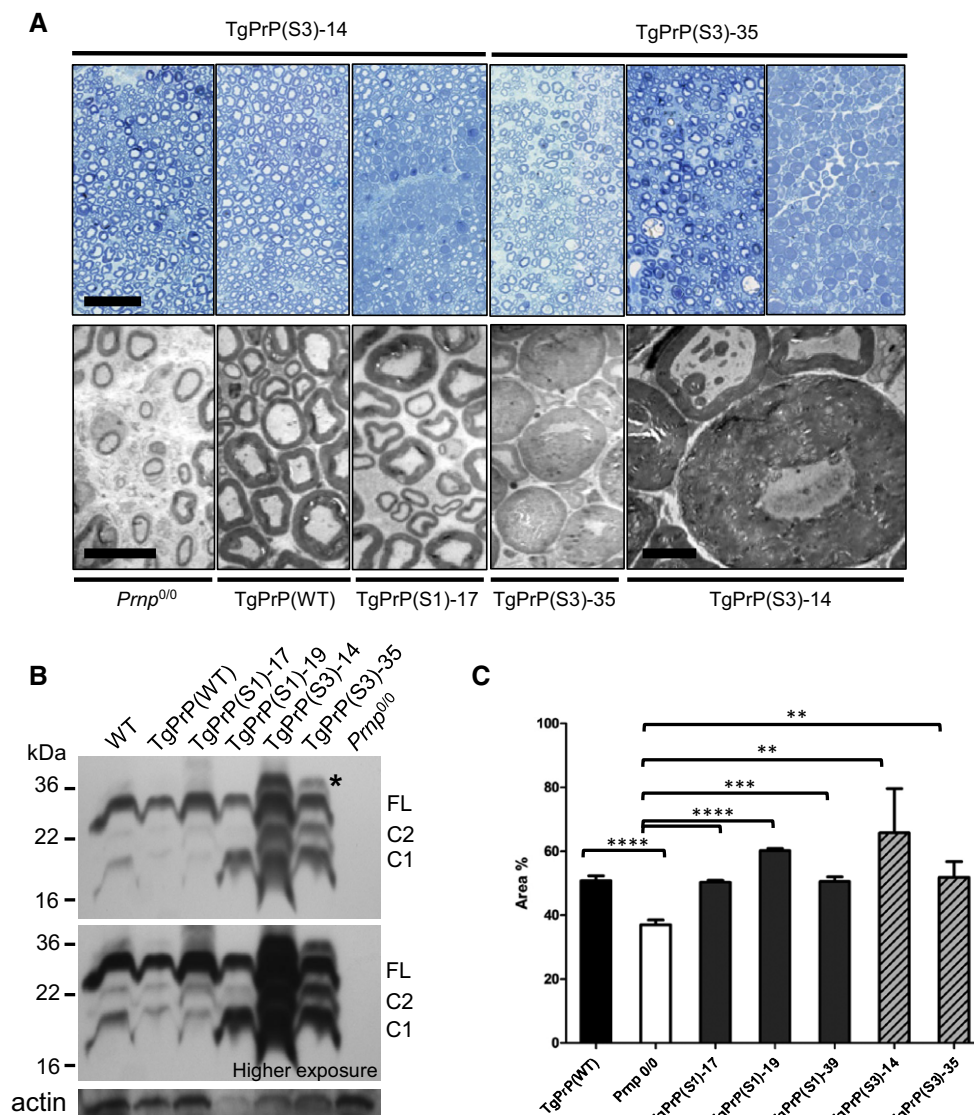
Figure 4. Variable rescue of the demyelinating polyneuropathy of $Prnp^{0/0}$ mice by the S3 PrP allele.

A Sections of sciatic nerve from TgPrP(S3.F88W)-14 female mice (all 610 days old) and TgPrP(S3.F88W)-35 female mice (614, 570 and 614 days old, respectively) were analysed using toluidine blue staining (upper row), with the third panels for each line showing a hypermyelinated phenotype. Scale bar in left panel represents 50 μm. The lower rows show EM analyses of mice of the indicated genotypes. Scale bar is 10 μm for panels 1–4, with the fifth panel showing a high power view to illustrate hypermyelinated fibres in a mouse expressing S3.F88W PrP (scale bar, 5 μm).

B Western blot analysis of sciatic nerve protein extracts (10 μg) from female mice after PNGaseF treatment shows a similar hierarchy of PrP expression in Tg lines to that of brain (see Fig 3). The asterisk indicates a greater than full-length fragment present in TgPrP(S3.F88W) mice, possibly corresponding to incomplete removal of the N-terminal signal peptide.

C Quantification of fibre morphology in aged animals (492–608 days old), representing the percentage of the nerve occupied by fibres versus the total cross-sectional area of the nerve. The S1 and S3.F88W alleles rescue $Prnp^{0/0}$ nerves to a similar percentage as the WT allele, but the variance and P-value is greater for the two Tg lines expressing the TgPrP(S3.F88W) allele. Unpaired, two-tailed t-test, **$P < 0.01$, ***$P < 0.001$, ****$P < 0.0001$. Sample sizes and exact P-values compared with $Prnp^{0/0}$ ($n = 9$) were as follows: TgPrP(WT) $n = 6$, $P = 3.63E-05$; $Prnp^{0/0}$, $n = 9$; TgPrP(S1)-17 $n = 5$, $P = 3.54E-05$; TgPrP(S1)-19 $n = 3$, $P = 6.35E-06$; TgPrP(S3.F88W)-14 $n = 3$, $P = 3.70E-03$; and TgPrP(S3.F88W)-35 $n = 7$, $P = 7.18E-03$.

Source data are available online for this figure.

S3.F88W PrP allele did not favour the appearance of a new prion strain with different pathological properties. Incubation times were longer than for direct passage into WT mice (164.3 ± 3.5 (SEM) versus 155.9 ± 2.0 days ($n = 12$, $n = 16$; $P = 0.05$)) and were consistent with a drop in titre measured by other techniques, as presented below.

**Profiling prions from infected TgPrP(S1) and TgPrP(S3.F88W) mice**

We carried out further analytical chemical procedures to increase our understanding of the pathogenic process in TgPrP(S1) and TgPrP(S3.F88W) mice. We separated protein species on the basis of

Table 2. Survival times for transgenic mice following intracerebral challenge with the RML isolate of mouse-adapted prions.

Mouse genotype	Genetic background	Mean survival ± SEM	N
TgPrP(S3.F88W)-35	FVB Prnp$^{0/0}$	84.1 ± 2.6	12
TgPrP(S3.F88W)-14	FVB Prnp$^{0/0}$	89.1 ± 2.5	16
TgPrP(S1)-17	FVB Prnp$^{0/0}$	139.1 ± 2.8	22
TgPrP(S1)-19	FVB Prnp$^{0/0}$	152.5 ± 2.5	17
TgPrP(S1)-39	FVB Prnp$^{0/0}$	424.4 ± 9.2	9
TgPrP(WT)	FVB Prnp$^{0/0}$	398.3 ± 8.1	12
WT	FVB	155.9 ± 2.0	16

size by velocity gradient fractionation of infected brain samples performed in the presence of the detergent sarkosyl. Next, the conformation-dependent immunoassay (CDI), which provides a signature of global protein folding via the accessibility of antibody epitopes, was used to assess the gradient fractions. Using these two technologies, and by performing analyses of gradient fractions in the presence or absence of proteinase K, we compiled an inventory of oligomeric PrP^{Sc} species: this inventory included net levels of protease-sensitive and protease-resistant (r) forms of PrP^{Sc} (rPrP^{Sc}), as well as PrP^C levels in fractions at the top of the gradients (Tables 1 and 3). As a prelude to these experiments, control analyses excluded the possibility that S1 and S3 allelic forms of PrP^C from uninfected mice had pre-existing conformational changes within the 12B2 antibody epitope used for CDI assays (Supplementary Fig S10). The sedimentation analyses showed a similar pattern of accumulation of PrP^{Sc} oligomeric species from RML-infected WT, TgPrP (S1) and TgPrP(S3.F88W) animals (Supplementary Fig S11). A different parameter, the denatured to native ratio of PrP^{Sc} (i.e. with and without exposure to 4 M GdnHCl; 'D/N ratio'), revealed subtle distinctions in the PrP^{Sc} populations in the brains of RML-infected
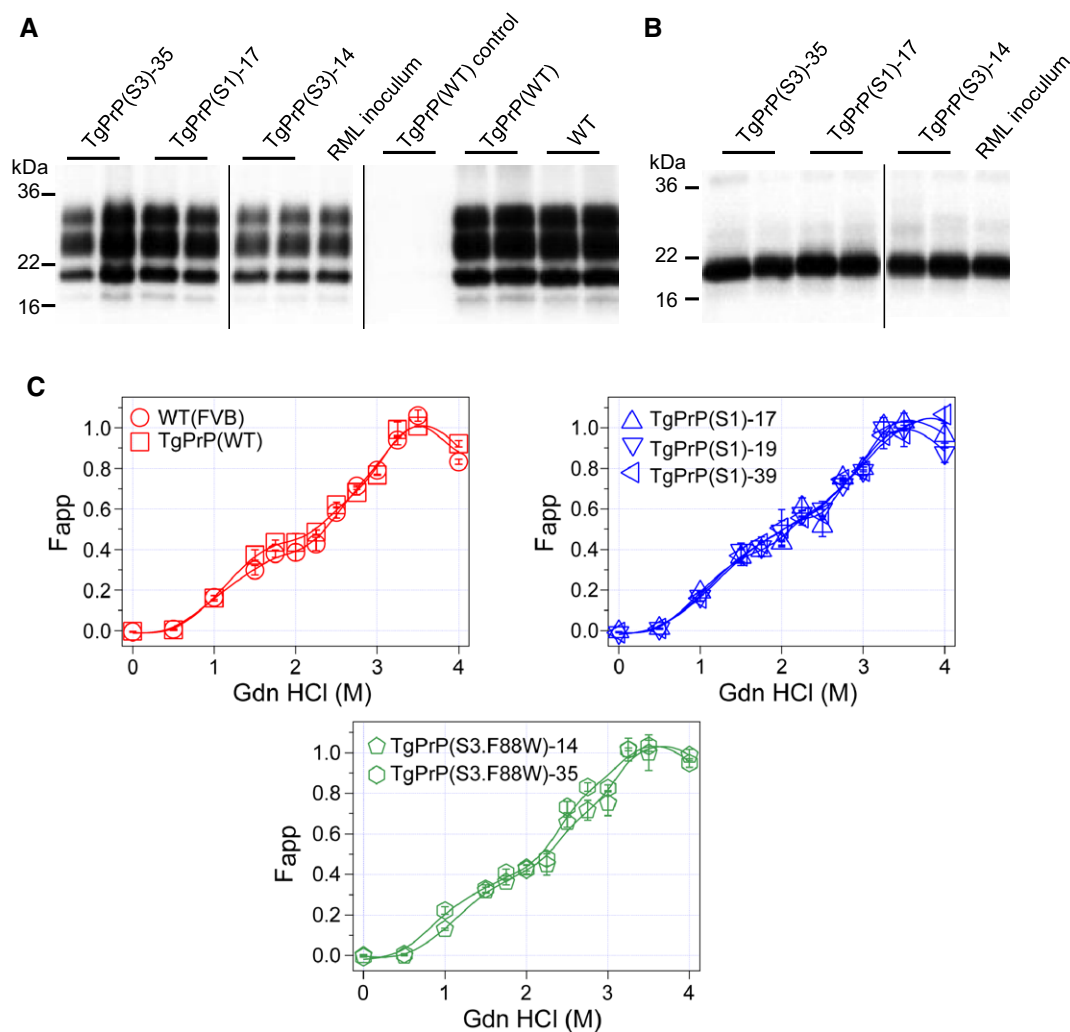
Figure 5. Biochemical properties of PrP^{Sc} from infected transgenic mice.

A, B   Infected brain homogenates were PK-digested and analysed by Western blot using (A) Sha31 antibody and (B) after PK and PNGaseF digestion using Sha31.

C   Conformational stability assay on RML-infected brain homogenates incubated with increasing concentrations of GdnHCl. The best-fit alignments of the data are presented. Genotypes are noted on the individual panels.

Source data are available online for this figure.

WT   TgPrP(S1)-19   TgPrP(S3)-35   WT

150 days   148 days   79 days ——→ 170 days
                                               ↓
                                           100 days
                                               ↓
                                           106 days ——→
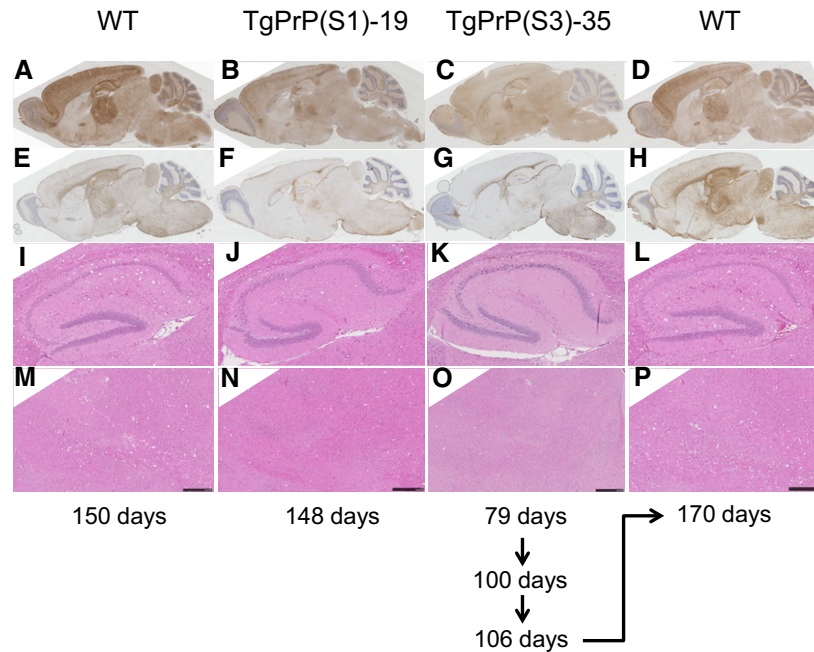
Figure 6.   Pathology of RML-infected mice.

A–H   The pattern of PrP^{Sc} deposition (A–D) and GFAP immunostaining (E–H) is presented.

I–P   A higher power view of H&E stained hippocampus (I–L) and thalamus (M–P) to reveal vacuolation is presented.

Data information: Animals of the same genotype are shown within a column, and incubation times of the presented animals with the RML prion isolate are shown (days). Mice expressing PrP S1 and S3 alleles (central columns) exhibit attenuated PrP^{Sc} deposition, gliosis and spongy change. Pathological features of the RML isolate are not altered upon sequential passage through TgPrP(S3.88W)-35 mice (see schematic at bottom of the diagram indicating sequential passages and finally, passage back into WT mice, compare the data in first and fourth columns).

Table 3.   PrP species from brain homogenates of prion-infected mice analysed by CDI after velocity centrifugation.

Mouse line[a]	PrP^C (ng/ml) ± SEM	PrP^{Sc} (ng/ml) ± SEM	rPrP^{Sc} (ng/ml) ± SEM	PrP^C/PrP^{Sc} ratio ± SEM	Incubation time (days) ± SEM
WT	757 ± 36.0	1769 ± 69	460 ± 8.1	1.6 ± 0.03	158 ± 5
TgPrP(WT)	274 ± 5.3	1101 ± 39	323 ± 13	0.8 ± 0.01	364 ± 11
TgPrP(S1)-17	414 ± 6	364 ± 18	110 ± 3	3.8 ± 0.06	139 ± 5
TgPrP(S1)-19	748 ± 13	589 ± 12	153 ± 4	4.9 ± 0.03	147 ± 1
TgPrP(S1)-39	172 ± 2.9	299 ± 4	82 ± 2	2.1 ± 0.01	411 ± 14
TgPrP(S3)-35	1408 ± 13.7	288 ± 5	107 ± 3	13.1 ± 0.10	74 ± 1
TgPrP(S3)-14	1816 ± 87.3	265 ± 8	94 ± 2	19.2 ± 0.39	91 ± 5

[a]All animals were infected with the RML isolate of mouse-adapted scrapie prions.

animals after PK treatment (Supplementary Fig S12). PrP^{Sc} derived from RML-infected WT (*Prnp*^{a}), TgPrP(S1)-17 and TgPrP(S1)-19 mice behaved in a similar manner with an increased D/N value after PK treatment, whereas PrP^{Sc} from infected TgPrP(S3.F88W)-14 and TgPrP(S3.F88W)-35 mice exhibited a drop in ratio. The assay used to obtain these data uses the 8H4 antibody for PrP capture and a Europium-labelled version of the 12B2 antibody for detection (with two epitopes located at residues 175–185 and 88–92, respectively). As alterations were not detected in the C-terminal protease-resistant core of PrP^{Sc} (Fig 5) and since a CDI signal is only generated if both epitopes are available, the drop in D/N ratio leads us to infer a shift in accessibility of the 12B2 epitope in rPrP^{Sc} populations of infected TgPrP(S3.F88W) mice.

Rather more notably, the CDI assay defined dramatic changes in quantities of protease-sensitive PrP^{Sc}, with infected TgPrP(S1) and TgPrP(S3.F88W) mice at disease endpoint both having lower levels than those of WT mice (Table 3, Supplementary Fig S12). For total PrP^{Sc} measured versus WT mice, there were averages of 4.2-fold and 6.4-fold reductions for TgPrP(S1) and TgPrP(S3.F88W) mice, respectively. Figures for the analogous reductions in protease-resistant PrP^{Sc} averaged across Tg lines of the same allelic type were 4.0× and 4.6×, respectively. These lower values for PK-sensitive PrP^{Sc} (and rPrP^{Sc}) were also paralleled by a drop in infectious titre as established by a homologous serial passage, which revealed a prolongation of incubation times (first passage 84.1 ± 2.6 days, $n = 12$ versus second passage 111.6 ± 3.8, $n = 5$, **$P = 0.0018$;

third passage 95.0 ± 0.6, $n = 5$, **$P = 0.0079$ versus second passage, *$P = 0.015$ versus first passage). Secondly, brain homogenates from primary passages into TgPrP(S1) and TgPrP(S3.F88W) mice generated significantly lower spot counts by the standard scrapie cell assay (SSCA; a technique to measure prion infectivity where a cell monolayer is infected with prions and eventually digested with PK to examine the number of cells with PrP^{Sc} and is in some respects similar to a plaque assay for viral particles (Klohn et al, 2003)) (Fig 7A). The reduction in titre of infectivity derived from TgPrP(S1) and TgPrP(S3.F88W) became more striking when the data were normalized for the extra levels of full-length PrP^C present in Tg versus WT mice.

While our data define a compromised ability to replicate RML prions in mice expressing S1 or S3 PrP, the shortened incubation periods in TgPrP(S3.F88W) mice stand in apparent contrast to this effect. To explore this effect and to accommodate the post-translational reduction in PrP^C that occurs during the course of disease (Mays et al, 2014), we plotted disease incubation times versus endpoint PrP^C:PrP^{Sc} ratios. Here, TgPrP(S1)-17, TgPrP(S1)-19 and TgPrP(S1)-39 lines plotted to a different regression from mice expressing different levels of the WT PrP^C allele (Prnp^a), while the TgPrP(S3.F88W)-14 and TgPrP(S3.F88W)-35 lines behaved in yet a third distinctive manner (Fig 7B), indicating unique pathogenic mechanisms operating in mice expressing the S1 and S3 PrP alleles. In sum, apart from the signature of denatured/native ratio, our CDI data did not reveal any qualitative differences in the nature of PrP^{Sc} in TgPrP(S1) and TgPrP(S3.F88W) mice; instead, repeated measures revealed drops in the quantities of protease-sensitive PrP^{Sc}, rPrP^{Sc}, infectious titre and associated neuropathology. Lastly, lower prion titre by SSCA (Fig 7A, $P < 0.001$) yet shorter incubation times (Table 2, $P = 2.44E-19$ and $1.75E-18$ in TgPrP(S3.F88W)-14 and TgPrP(S3.F88W)-35 mice, respectively) versus WT mice indicates an uncoupling effect such that these Tg animals respond to pathologic forms of PrP differently from their WT counterparts (Fig 7C), as discussed below.

Discussion

### β-processing of PrP^C directed by a variant octarepeat region

An unexpected result in our study of OR function was that the expression of mutant PrP associated with component 3 geometry (i.e. the S3 and S3F88W PrP alleles) in RK13 cells or Tg mice resulted in a ~3.5-fold elevated level of a ~20–21 kDa C2 fragment. A reciprocal trend for decreased C2 production by S1 alleles (Table 1) did not reach significance. The increased C2 levels observed in our experiments cannot be attributed to differential turnover effects as S3 PrP and WT PrP have identical amino acid sequences for this fragment (see Fig 1); instead, the effect is attributed to increased cleavage. Though Tg mice expressing S3 PrP have increased levels of full-length PrP compared to WT, this alone does not account for the increased levels of C2 fragment as uninfected tga20 mice overexpressing PrP six-fold do not over-produce the C2 fragment (Fischer et al, 1996; Westergard et al, 2011). While protease-sensitive C2 is present in uninfected cells (Mange et al, 2004) and accumulates in infected animals, there is comparatively little known about its genesis in vivo. With

recombinant PrP (McMahon et al, 2001) and with additives to cultured cells (Watt et al, 2005), there is a relationship to reactive oxygen species, but our cumulative data indicate that increased C2 production from S3 alleles is unlikely to be a direct effect of Cu-binding within the OR, as suggested by previous in vitro studies (McMahon et al, 2001; Pushie & Vogel, 2008, 2009). The possibility that ablation of OR metal binding by HoctaY substitutions delegates activity to the adjacent metal-binding site, 'site 5', involving H95 and H110 residues (Jackson et al, 2001; Kramer et al, 2001; Qin et al, 2002) was excluded by a compound mutated allele composed of OR HoctaY + H95A, which still exhibited robust production of the C2 fragment (Fig 2B).

Although prolines play a key role cuing the S3 PrP allele for C2 proteolysis (Figs 1C and 2C), two observations argue that this effect does not arise simply from an enzymatic preference for these residues. First, while there is a CNS-expressed protease with a preference for cleaving after prolines, the nature of the beta-propeller structure guarding the active site in prolyl endopeptidase means (as its alternative name prolyl oligopeptidase suggests) that peptides are preferred over polypeptides as substrates (Szeltner & Polgar, 2008). Second, preliminary mass spectrometry studies of PrP^C immuno-precipitated from brain and cleaved chemically at Met128 reveal no prolines in positions immediately N-terminal to C2-like fragments. Instead, the PrP fragments with confident assignments are the same in TgPrP(S3.F88W) mice and Tga20 mice expressing WT PrP^C (G. Schmitt-Ulms, personal communication). Thus, S3 PrP is likely processed by the same protease that processes WT PrP^C.

Enhanced C2 generation by the S3 allele appears to reflect a facet of N-terminal domain function that is not related to the nature of amino acid residue side chains, but that is impacted by the flexibility of the polypeptide backbone. Proline is a unique component of polypeptides with partial double-bond character in the carbon–nitrogen backbone (between the nitrogen of the ring structure and proceeding carbon atom with a carbonyl group) that restricts free rotation. While two GQ > PP substitutions in the S1 PrP allele had no effect upon C2 production (Figs 1–3), single G > P substitutions in ORs 2–5, GGG -> GPG, appear crucial for scission of S3 PrP (Fig 2B) and distinguish this effect functionally and structurally from a potential role of the adjacent tryptophan-glycine (WG) motifs, which may affect RNA processing events (Gibbings et al, 2012). The role of single proline residues in facilitating cleavage is exemplified by experiments to introduce GPG motifs one-by-one into the GGG sequences of octarepeats 5, 4, 3 and 2, which causes a ladder of increments in the length of the C2 fragment (Fig 2C). As increased C2 production is not joined by a similar increase in C1 production, there is a consequent alteration in the C2:C1 ratio. Since TgPrP(S3.F88W) mice with altered C2:C1, in turn, behave in a singular manner for some biological endpoints (below), determining the exact mechanism of chain scission—presumably mediated by a protease with tissue-specific distribution—will be an important future goal. Furthermore, since C2 PrP contains the major binding site for oligomeric forms of Aβ (Lauren et al, 2009), β-processing of PrP may have ramifications that extend to AD pathogenesis.

Lastly, by way of clarification, supraendogenous levels of C2 PrP are observed in prion infections (Chen et al, 1995; Yadavalli et al, 2004). In this context, C2 PrP resembles the core of the infectious prion protein PrP27–30 that is PK resistant, while C2 derived from PrP^C remains PK sensitive (Mays et al, 2014) (Supplementary Table
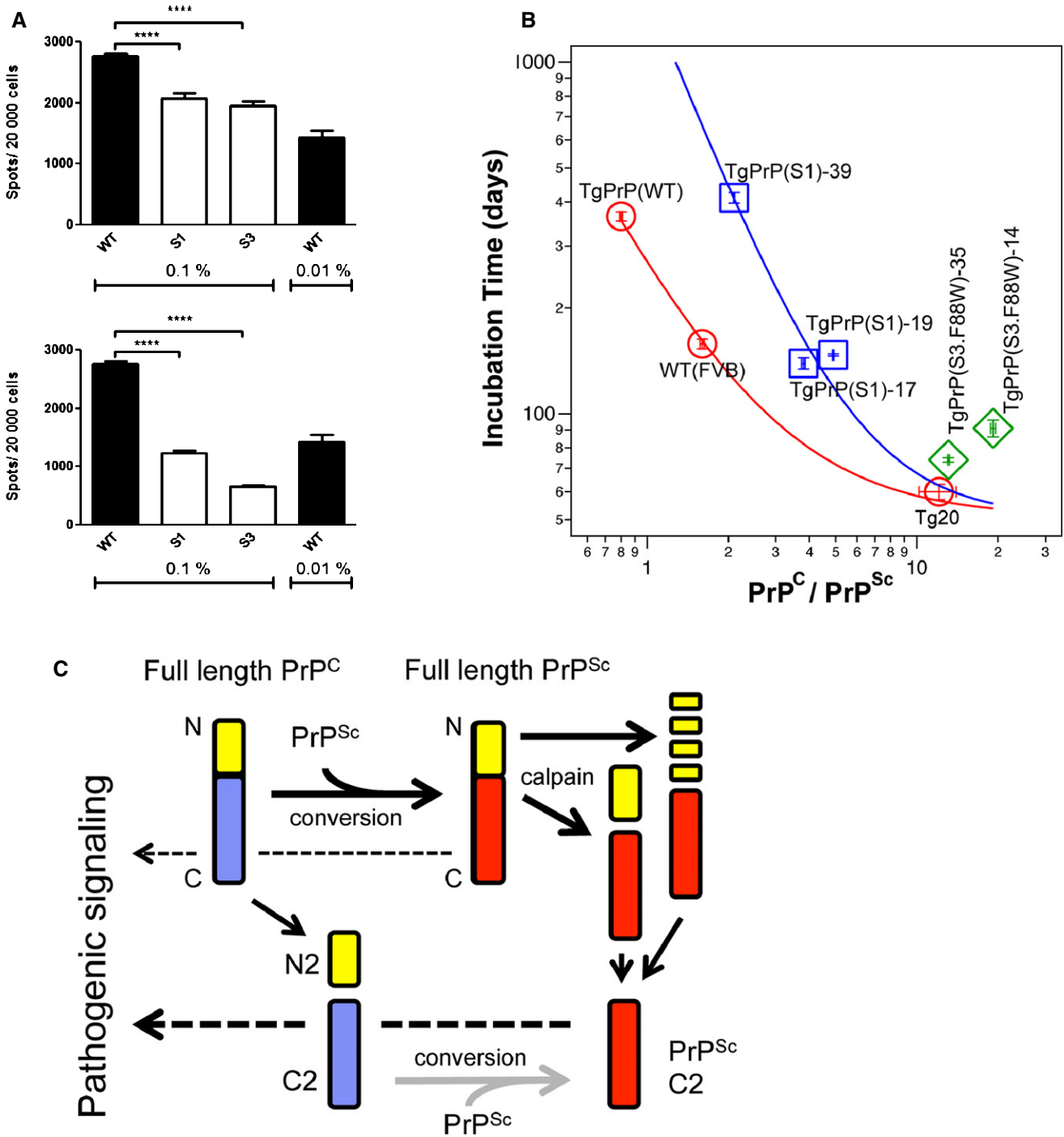
Figure 7. Biochemical properties of PrP^{Sc} assessed by guanidine denaturation and CDI.

A   Spot counts in the scrapie cell assay using WT, TgPrP(S1)-17 and TgPrP(S3.F88W)-14 brain homogenates (0.1% or 0.01%) from mice infected with RML are shown in the upper panel (WT vs S1 P = 2.09E-05 and vs S3 P = 4.62E-08) with numbers corrected for PrP^C expression levels as per Table 1 presented in the lower panel (WT vs S1 P = 1.04E-13 and vs S3 P = 3.39E-20; two-tailed t-test, n = 3).

B   A comparison of incubation time vs PrP^C:PrP^{Sc} ratio for mice expressing different levels of WT PrP (WT, TgPrP(WT), tga20), S1 PrP (TgPrP(S1)-17, TgPrP(S1)-19, TgPrP(S1)-39) and S3 PrP (TgPrP(S3.F88W)-14, TgPrP(S3.F88W)-35).

C   Formation and biological activities of PrP species. Synthetic and proteolytic pathways are shown from left to right, while pathways for pathologic signalling from PrP^{Sc} through PrP^C and PrP^C-derived fragments are shown from right to left (dashed arrows). Alternative pathways to remove N-terminal sequences (yellow) from the protease-resistant C-terminal Core (red) in infected cells are shown, while N2 is removed from a protease-sensitive C-terminal core (blue) in healthy cells. Grey arrow indicates that formation of PrP^{Sc} C2 from protease-sensitive C2 is not particularly efficient as mice with high levels of C2 are not more efficient in synthesizing PrP^{Sc}. Heavy dashed arrow through protease-sensitive C2 indicates that this species may be adept at pathogenic signalling as mice with lower PrP^{Sc} burden than WT mice succumb to disease earlier. For simplicity, physiological signalling pathways through PrP^C species are not shown.

S1). This type of C2 PrP may arise from a processive protease activity often referred to as 'N-terminal trimming' and attributed, at least in cells, to the action of lysosomal proteases (Taraboulos et al, 1992). The Ca^{2+}-activated non-lysosomal protease calpain has also been invoked for the production of this species (Yadavalli et al, 2004). Whether the ultimate effect of C2 PrP on infection differs depending on the mechanism of production remains to be determined.

Prion replication and pathogenesis in TgPrP(S1) and TgPrP (S3.F88W) mice

Transgenic studies have shown an unambiguous requirement for PrP^C C-terminal sequences to support efficient prion propagation (Fischer et al, 1996; Supattapone et al, 1999; Flechsig et al, 2004), but there is a growing appreciation that the N-terminal natively unstructured region contains targeting signals that impact the eligibility of PrP^C substrates (Sunyach et al, 2003) and also undergoes cis interactions with distal sequences (Flechsig et al, 2000; Qin et al, 2000; Sonati et al, 2013; Spevacek et al, 2013). In earlier studies, deletions that remove all or part of the OR (PrPΔ32–80, PrPΔ69–84) were associated with a ten-fold drop in titre and a four-fold drop in protease-resistant PrP^{Sc} (Fischer et al, 1996). PrPΔ32–93 deletion alleles were associated with a 10–30× drop in titre and 30–50× drop in PrP^{Sc} precipitated with sodium phosphotungstate, and no overt CNS pathology (Flechsig et al, 2000). Studies described here also caused drops in levels of misfolded PrPs but did not perturb PrP residues 32–50 which contain a different type of motif, namely two hexarepeats (Flechsig et al, 2000). Instead, we used missense mutations restricted to the OR region (residues 50–90 in mouse) to gain insights into the function of this enigmatic domain within the context of full-length PrP^C molecules.

For both the S1 and S3 PrP alleles, with the single exception of altered denatured/native ratios for S3 (Supplementary Fig S12), we were unable to discern allelic differences in the quality of protease-resistant forms of PrP using gel electrophoresis, GdnHCl denaturation and sedimentation profiling of oligomeric species (Fig 5, Supplementary Figs S9 and S11). Quantitative changes were apparent, however.

For S1 PrP, while expressed at higher than endogenous WT levels in both the TgPrP(S1)-17 and TgPrP(S1)-19 lines, PrP^{Sc} isoforms at disease endpoint (Table 3, Supplementary Fig S11) and spot counts in SSCA (Fig 7A) were depressed. We can conclude that S1 PrP is less efficient than WT PrP^C in the tempo and ceiling value for production of total PrP^{Sc}, rPrP^{Sc} and prion titre. These data therefore extend earlier genetic studies that deleted the OR and flanking sequences (Fischer et al, 1996; Flechsig et al, 2000) by defining the competence for chain flexibility in the OR as a factor that allows for accumulation of prion titre, total PrP^{Sc} and rPrP^{Sc} to attain WT levels.

In the case of S3 PrP, the Tg mice expressing this allele succumbed to prion disease ~60 days earlier than TgPrP(S1)-17 and TgPrP(S1)-19 mice. Two variables are relevant in drawing these comparisons: the levels of full-length PrP^C in uninfected TgPrP(S3.F88W)-14 and TgPrP(S3.F88W)-35 mice are increased 0.7× over TgPrP(S1)-17 and TgPrP(S1)-19 mice, while the ratio of C2 production changes by greater than three-fold (Table 1). Regarding the former, it is well known that increasing full-length PrP^C above WT levels decreases disease duration (Carlson et al, 1994). In the case of mice expressing WT PrP at 3–4× levels, incubation times with the same RML prion isolate were 100 ± 17 days (Fischer et al, 1996) versus 89.1 ± 2.5 and 84.1 ± 2.6 days in the TgPrP(S3.F88W)-14 and TgPrP(S3.F88W)-35 lines with 3× expression, respectively (Tables 1 and 2); these figures are in reasonable agreement given the margins of error in scoring the terminal phase of prion disease and could suggest that expression level is the key variable in arriving at incubation times < 100 days. However, quite curiously, S3 PrP alleles also have levels of pathogenesis-associated species that are below those of WT controls; lower spot counts in SSCA (Fig 7A); a four-fold drop in rPrP^{Sc}; and a > six-fold drop in protease-sensitive PrP^{Sc} isoforms at disease endpoint (Table 3, Supplementary Fig S11). Our studies also found a prolongation of incubation time period upon passage through TgPrP(S3.F88W)-35 mice but the drop in infectious titre that did not reach significance (noting that a one log-unit drop defines a minimum for a significant change in titre determined by bioassay (Prusiner, 1987)). To resolve the paradox of lower amounts of pathogenic species yet abbreviated incubation times, we infer that C2 PrP—normally present at much lower levels than C1 PrP—may be important and have a greater ability to perform signalling from pathogenic forms of PrP (Fig 7C). Future experiments with knock-in mice and ex vivo cultures may be of great use to tease apart the relationships between truncated PrP^C species and toxic signalling originating from PrP^{Sc} or Aβ oligomers.

Octarepeat region binding partners and uncoupling of disease phenotypes

We redesigned the PrP OR with an expectation that biological properties of the conformationally locked S1 and S3 alleles would differ from WT PrP—this expectation was fulfilled for aspects of disease pathogenesis and for some aspects of a physiological function in maintaining myelination of peripheral nerves (Figs 3, 4, 6 and 7), thus confirming a modulatory function for the OR. The effects ascertained in infected TgPrP(S1) and TgPrP(S3.F88W) mice are of special interest because uncoupling between neurological disease and accumulation of PrP^{Sc} has been seen previously, and at one stage, it was used to argue against the validity of the prion hypothesis that the infectious agent is composed of misfolded PrP (Czub et al, 1986; Lasmezas et al, 1997). While disease transmission from recombinant PrP molecules address the latter issue (Legname et al, 2004; Wang et al, 2010), data presented here now begin to suggest a mechanistic basis for how uncoupling might occur, namely by modulating OR rigidity.

From our studies using amino acid substitutions to perturb OR rigidity, we deduce that altered interactions with OR-binding cofactors that vary within the physiological environment will also modulate OR rigidity and consequently affect roles of the PrP linker region and globular domain in prion replication and pathogenic signalling from PrP^C (Brandner et al, 1996; Spevacek et al, 2013). While our initial focus has been copper binding, the WT OR can bind other species (Beland & Roucou, 2012). Binding partners with repetitive structures can make multiple contacts within the OR, and one molecule that holds the OR in an extended conformation, pentosan sulphate, is a potent inhibitor of prion accumulation (Taubner et al, 2010); in studies here, an extended conformation, 'component 1' geometry is inferred for the S1 PrP allele (Fig 1B). In the case of the S3 PrP allele tailored for a compact OR conformation, the

mechanism of pathogenesis may be different and might encompass altered susceptibility to β-cleavage occurring as a consequence of altered OR rigidity. In sum, the pleiotropic effects of proline substitutions that limit OR flexibility can be reconciled with this domain serving as a cell surface scaffold to bind diverse macromolecules and co-factors.

Beyond prion infections, the clinical onset of genetic prion diseases varies greatly, even when the effects of a common *PRNP* codon 129 polymorphism on the disease chromosome and on the non-mutated chromosome are excluded from the analyses. For example, corrected data on the P102L mutation in the PrP^C linker region define an average age of onset of 46.8 years with a standard deviation 12.4 years (Mead *et al*, 2006). Within an extended kindred with six extra octarepeats and early disease onset, the codon 129 genotype accounted for only 41% of the variance (Mead *et al*, 2006). Since our studies define OR flexibility as impacting diverse biological endpoints, we suggest it will prove to be an important variable in infectious disease paradigms where levels of PrP^Sc and infectivity appear dissociated from the onset of clinical disease. More generally, the OR can be likened to a clutch that controls the degree to which abnormally folded PrPs engage or disengage mechanisms to drive neurological disease. This action may also apply to familial prion diseases where a single mutant allele is capable of producing multiple clinical presentations.

Materials and Methods

Mutant PrP plasmid constructs

To create novel alleles in the PrP OR equivalent to the synthetic peptides (sequences available in Supplementary Materials and Methods) examined by electron paramagnetic resonance (EPR) spectroscopy (Supplementary Fig S1), the sequences encoding the N-terminal portion (with the mutations included) of PrP and part of the 5' UTR were synthesized by GenScript Inc. The cassettes encoding the OR-encoding sequences of interest were excised from the plasmid provided by GenScript using *KpnI* (New England Biolabs), annealed into the full-length PrP sequences in an existing pCDNA3 plasmid using T4 DNA ligase (New England Biolabs), and correct full-length PrP sequences were then moved into another vector pBudgfp by digestion with *XbaI* and *HindIII* (New England Biolabs), followed by gel extraction and ligation. For phenylalanine substitutions into the hydrophobic domain, proline substitutions into the octarepeats (G62P, G70P, G78P, G86P) and H95A mutations, primers were designed as per the GeneTailor Site-Directed Mutagenesis kit (Invitrogen) and the mutagenesis reaction was carried out as per the manufacturer's protocol. One microlitre of each reaction was transformed into competent DH5α cells (Invitrogen), and plasmids were isolated using a miniprep kit (Qiagen). Correct plasmids were confirmed by sequencing.

Cell culture

Rabbit kidney epithelial (RK13), neuroblastoma (N2a), cured SMB (SMB-PS), human kidney epithelial (HEK) and human neuroblastoma (SH-SY5Y) cells were maintained in Dulbecco's modified Eagle's medium (DMEM; Invitrogen) supplemented with 10% foetal bovine serum (FBS; Invitrogen) and penicillin/streptomycin (Invitrogen) at 37°C and 5% CO_2 levels. Cells of approximately 90–100% confluency were transfected using Lipofectamine 2000 (Invitrogen), according to the manufacturer's instructions. RK13 cell lines stably expressing wild-type (WT) PrP (WT-10) and mutant S1 (S1–29), S3 (S3–27) and S3.F88W (F88W-5) PrP were created by transfection with plasmids encoding the proteins, and clones were selected using zeocin (Invitrogen). Clones isolated with cloning rings (Scienceware) were amplified, lysed with RIPA buffer (50 mM Tris–HCl pH 7.5, 150 mM NaCl, 0.5% sodium deoxycholate, 1% NP-40) and analysed by Western blot for PrP expression.

Transgenic mouse lines

For the generation of transgenic mice, sequences encoding WT PrP and mutant S1 and S3.F88W PrP were inserted into the MoPrP.*Xho* 'half-genomic' vector (Borchelt *et al*, 1996; Fischer *et al*, 1996). Mutant PrP sequences were extracted from the mutant PrP plasmids described above using the primers 5′AAAAACTCGAGGCCCTCA TCCCACGATCAGG3′ and 5′AAAAACTCGAGAGTCCAATTTAGGAG AGCCAAG3′, which contain *XhoI* restriction enzyme sites. Polymerase chain reaction (PCR) fragments were cloned into pCR2.1.TOPO (Invitrogen), and sequences were verified. DNA from TOPO clones was digested using *XhoI* (New England Biolabs), isolated by gel electrophoresis and purified with a gel extraction kit (Qiagen). The MoPrP.*Xho* vector was digested with *XhoI*, treated with calf intestinal alkaline phosphatase (New England Biolabs), phenol: chloroform-extracted and ethanol-precipitated or purified with the Ultraclean Gel Spin DNA Purification Kit (MoBio Laboratories). After ligation of digested fragments, the sequenced DNA was amplified and purified using the Endo-Free Maxiprep Kit (Qiagen). To prepare for injection, the DNA was digested with *NotI* and purified using the gel extraction kit (Qiagen) or Ultraclean Gel Spin DNA Purification Kit (MoBio Laboratories). The DNA was then injected into the pronuclei of mouse FVB embryos by the University of Calgary Transgenic Services.

Tissue homogenate preparation, gradient fractionation, CDI and SSCA

Ten per cent homogenates (w/v) of brain, spleen, heart, kidney, liver and lung were prepared in PBS complemented with Complete Mini Protease Inhibitor (Roche) using a homogenizer (VWR, model VDI 12) at 4°C. Sucrose gradient and the conformation-dependent immunoassay (CDI) were performed as previously described (Kim *et al*, 2012). Briefly, the 400-μl aliquots of 10% brain homogenate in PBS, pH 7.4, containing 2% sarkosyl were clarified by centrifugation at 500 *g* for 5 min and carefully layered onto the top of the 10% to 45% sucrose gradient prepared in PBS, pH 7.4, containing 1% sarkosyl. Ultracentrifugation was performed at 237,000 *g* for 73 min at 5°C in an Optima TL ultracentrifuge (Beckman) equipped with a Beckman SW 55 Ti rotor. After the centrifugation, fractions were collected from the bottom of the tube. The CDI assay was similar to previous descriptions (Safar *et al*, 2005; Choi *et al*, 2009) albeit with incorporation of several recent modifications (Mays *et al*, 2014). The standard scrapie cell assay (SSCA) was performed as described using L929 cells (Mays *et al*, 2014).

Western blotting

Samples were run on 12% or 14% Tris-glycine gels using a Bio-Rad system and transferred to polyvinyl difluoride (PVDF; Millipore) membranes. Blots were immediately incubated with PrP antibody Sha31 (Spi-Bio Inc; 1/30,000 in 0.5% TBST) or were blocked with 5% skim milk in 0.1% TBST for 1 h at room temperature and incubated with primary antibody at 4°C overnight (PrP antibodies: 9A2 1/4,000, 12B2 1/8,500, SAF83 (Cayman), VRQ61 1/5,000, and 2D6 1/10,000, 1A6 1/5,000). 9A2 and 12B2 were gifts from Dr. Jan Langeveld (Langeveld *et al*, 2006), VRQ61 and 2D6 from Dr. Human Rezaei (Moudjou *et al*, 2004), and 1A6 was produced in-house. Membranes were subsequently incubated with secondary antibody at 1/10,000 (Bio-Rad) for 2 h at room temperature and visualized using ECL (Pierce). After stripping, membranes were incubated in anti-actin primary antibody (Sigma; 1/5,000).

Proteinase K and PNGaseF digestion

Samples were treated with 50 μg/ml of proteinase K (PK; Invitrogen) for 1 h at 37°C. The reaction was stopped with 2 mM phenylmethanesulfonyl fluoride (PMSF) and centrifuged at 13,000 rpm for 1 h at 4°C. The pellets were resuspended in 15 μl PBS and 3 μl of 6× SDS loading buffer was added before boiling. If samples were to undergo further PNGaseF digestion, the pellets were resuspended in 15 μl of 2% SDS and heated at 100°C for 10 min. Two microlitres of 10% NP-40, 2 μl of 10× G7 Reaction Buffer and 1 μl of PNGaseF were added, and the reaction was incubated at 37°C for 2 h. The reaction was stopped by adding 6× SDS loading dye and boiling. Samples not PK digested were digested by PNGaseF according to the manufacturer's protocol, overnight at 37°C with 0.2 μl of PNGaseF.

Guanidine hydrochloride denaturation of PrP^Sc

The 10% brain homogenate was centrifuged at 700 *g* for 5 min, and the supernatant was collected. Equal amounts of brain homogenate were added to increasing concentrations of guanidine hydrochloride (GdnHCl) (Sigma), and the samples were shaken at 800 rpm for 2 h at room temperature. The concentration of GdnHCl was diluted to 0.4 M using RIPA buffer, and the total volume of each sample was made equal by adding 0.4 M GdnHCl. Samples were treated with 50 μg/ml PK for 1 h at 37°C, and the reaction was stopped using PMSF (1 mM final concentration). The samples were centrifuged at 100,000 *g* at 4°C, the pellet was resuspended in PBS, and 6× SDS loading buffer was added.

Mouse inoculations, scoring and sample collection

Animals were housed in ventilated cages with a 12-h light/dark cycle and were given *ad libitum* access to food and water. Male and female FVB mice 4–7 weeks of age were randomly assigned for inoculation with RML (source S. Prusiner), natural scrapie from a Canadian ARQ/ARQ sheep (CFIA, Nepean, ON), classical BSE from a Canadian animal (CFIA, Nepean, ON), or uninfected WT mouse brain homogenate (control). Approximate sample sizes for each group were determined by previous inoculation experiments in the literature. Thirty microlitres of 1% brain homogenate in PBS was

The paper explained

Problem
Prion diseases are fatal neurodegenerative diseases where a key feature is spongiform change in the brain. One of the basic processes involved is the conversion of the cellular form of the prion protein (PrP^C) to an infectious form PrP^Sc. There are no therapeutics currently available due to the lack of understanding of the basic mechanisms involved in the disease. Although the C-terminus of PrP^C is required for disease to occur, relatively little is known about the impact of the N-terminus.

Results
We find that the flexibility of the octarepeat region in the N-terminus of PrP^C that binds transition metals such as copper is a crucial determinant in disease. Using PrP mutants where the octarepeat region is locked into specific conformations, we found that we could uncouple the production of PrP^Sc and infectivity from pathogenesis in that lower titres of PrP^Sc were observed with a faster onset of disease. Furthermore, we observed increased endoproteolysis of PrP^C into the C2 fragment. Thus, the N-terminus of PrP^C is able to affect various facets of prion disease including endoproteolysis, PrP^Sc production and pathogenesis.

Impact
Our study underlines the importance of structure in the N-terminus of PrP^C on the pathogenesis of prion diseases and establishes new reagents to analyse disease pathogenesis and therapeutic strategies.

injected using a 25-gauge needle into the parietal lobe of each mouse. The inoculum was heated for 20 min at 80°C before inoculations were performed. After inoculations, mice were checked for symptoms of prion disease, including head tilt, ataxia, extension, clasp, weight loss and stupor; initial diagnosis of clinical disease onset was performed by animal staff performing health monitoring. Animals euthanized due to non-prion disease-related illness or injury were excluded from analyses. Animal experiments were performed in accordance with the Animal Care Committee of the University of Alberta, protocols AUP00000356 and AUP00000357.

Immunohistochemistry and image analysis

Brains were fixed in 10% formalin for 48 h and were subsequently paraffin-embedded. Sections 4.5–6 μm thick underwent standard de-paraffinization and hydration, were treated with 4 M guanidine thiocyanate and probed for PrP^Sc using SAF83 antibody. Glutaraldehyde-fixed samples of sciatic nerve were processed as described previously (Westaway *et al*, 1994), with bright-field images of nerve cross sections captured with a 10× objective (Nikon Eclipse 90i microscope). GE Healthcare Investigator software was used to analyse individual nerves for area, circumference and fibre count (see Supplementary Materials and Methods).

Electron microscopy and toluidine staining

Sciatic nerves fixed in 2% glutaraldehyde/1% paraformaldehyde and post-fixed in 1% osmium tetroxide were Epon-embedded using routine procedures, and ultrathin sections were cut. Semi-thin sections (0.5 μM) were used for toluidine blue staining, and ultrathin

sections were used for electron microscopy. The ultrathin sections were mounted on formvar-coated copper grids and contrasted with uranyl acetate and lead citrate. The samples were viewed in a Jeol JEM-2100 electron microscope at an acceleration voltage of 120 kV and a magnification range of 1,500× to 4,000×. Electron micrographs were recorded on a Gatan Erlangshen ES500W CCD camera.

Statistics

Normal distribution of data was confirmed by a Kolmogorov–Smirnov test, and unpaired, two-tailed Student's *t*-tests were used for comparisons of these sample groups with no *a priori* predictions for the performance of the PrP alleles. For incubation time data with $n < 6$ where normal distribution could not be confirmed, we used a Mann–Whitney test. Statistical tests were performed using InStat and GraphPad Prism software with *P*-values < 0.01; < 0.001 and < 0.0001 represented by 2, 3 or 4 asterisks, respectively. Exact *P*-values are reported in the main text or the figure legends and were calculated using GraphPad Prism and Microsoft Excel.

Author contributions

Experiments were designed by AL, AM, GLM and DW. Experiments were performed and analysed by AL, AM, ND, CEM, EDW, RA, RCCM, SW, JY, BS, JVM, HG, CK, HW, AB, GSU, JGS, GLM and DW. The mouse colony was maintained by JY and JG. The manuscript was written by AL and DW.

Conflict of interest

The authors declare that they have no conflict of interest.

For more information

http://www.cjdfoundation.org

http://www.prioninstitute.ca

References

Aguzzi A, Falsig J (2012) Prion propagation, toxicity and degradation. *Nat Neurosci* 15: 936–939

Beland M, Roucou X (2012) The prion protein unstructured N-terminal region is a broad-spectrum molecular sensor with diverse and contrasting potential functions. *J Neurochem* 120: 853–868

Benilova I, Karran E, De Strooper B (2012) The toxic Abeta oligomer and Alzheimer's disease: an emperor in need of clothes. *Nat Neurosci* 15: 349–357

Borchelt DR, Davis J, Fischer M, Lee MK, Slunt HH, Ratovitsky T, Regard J, Copeland NG, Jenkins NA, Sisodia SS *et al* (1996) A vector for expressing foreign genes in the brains and hearts of transgenic mice. *Genet Anal* 13: 159–163

Brandner S, Isenmann S, Raeber A, Fischer M, Sailer A, Kobayashi Y, Marino S, Weissmann C, Aguzzi A (1996) Normal host prion protein necessary for scrapie-induced neurotoxicity. *Nature* 379: 339–343

Bremer J, Baumann F, Tiberi C, Wessig C, Fischer H, Schwarz P, Steele AD, Toyka KV, Nave KA, Weis J *et al* (2010) Axonal prion protein is required for peripheral myelin maintenance. *Nat Neurosci* 13: 310–318

Bueler H, Raeber A, Sailer A, Fischer M, Aguzzi A, Weissmann C (1994) High prion and PrPSc levels but delayed onset of disease in scrapie-inoculated mice heterozygous for a disrupted PrP gene. *Mol Med* 1: 19–30

Carlson GA, Ebeling C, Yang S-L, Telling G, Torchia M, Groth D, Westaway D, DeArmond SJ, Prusiner SB (1994) Prion isolate specified allotypic interactions between the cellular and scrapie prion proteins in congenic and transgenic mice. *Proc Natl Acad Sci USA* 91: 5690–5694

Chattopadhyay M, Walter ED, Newell DJ, Jackson PJ, Aronoff-Spencer E, Peisach J, Gerfen GJ, Bennett B, Antholine WE, Millhauser GL (2005) The octarepeat domain of the prion protein binds Cu(II) with three distinct coordination modes at pH 7.4. *J Am Chem Soc* 127: 12647–12656

Chen SG, Teplow D, Parchi P, Gambetti P, Autilio-Gambetti L (1995) Truncated forms of the human prion protein in normal brain and in prion diseases. *J Biol Chem* 270: 19173–19180

Chiarini LB, Freitas AR, Zanata SM, Brentani RR, Martins VR, Linden R (2002) Cellular prion protein transduces neuroprotective signals. *EMBO J* 21: 3317–3326

Choi EM, Geschwind MD, Deering C, Pomeroy K, Kuo A, Miller BL, Safar JG, Prusiner SB (2009) Prion proteins in subpopulations of white blood cells from patients with sporadic Creutzfeldt-Jakob disease. *Lab Invest* 89: 624–635

Colby DW, Wain R, Baskakov IV, Legname G, Palmer CG, Nguyen HO, Lemus A, Cohen FE, DeArmond SJ, Prusiner SB (2010) Protease-sensitive synthetic prions. *PLoS Pathog* 6: e1000736

Collinge J, Clarke AR (2007) A general model of prion strains and their pathogenicity. *Science* 318: 930–936

Czub M, Braig HR, Diringer H (1986) Pathogenesis of scrapie: study of the temporal development of clinical symptoms of infectivity titres and scrapie-associated fibrils in brains of hamsters infected intraperitoneally. *J Gen Virol* 67: 2005–2009

Dron M, Moudjou M, Chapuis J, Salamat MK, Bernard J, Cronier S, Langevin C, Laude H (2010) Endogenous proteolytic cleavage of disease-associated prion protein to produce C2 fragments is strongly cell- and tissue-dependent. *J Biol Chem* 285: 10252–10264

Feraudet C, Morel N, Simon S, Volland H, Frobert Y, Creminon C, Vilette D, Lehmann S, Grassi J (2005) Screening of 145 anti-PrP monoclonal antibodies for their capacity to inhibit PrPSc replication in infected cells. *J Biol Chem* 280: 11247–11258

Fischer M, Rulicke T, Raeber A, Sailer A, Moser M, Oesch B, Brandner S, Aguzzi A, Weissmann C (1996) Prion protein (PrP) with amino-proximal deletions restoring susceptibility of PrP knockout mice to scrapie. *EMBO J* 15: 1255–1264

Flechsig E, Manson JC, Barron R, Aguzzi A, Weissmann C (2004) Knockouts, Knockins, Transgenics and Transplants in Prion Research. In *Prion Biology and Diseases*, Prusiner SB (ed). , pp 373–434. Cold Spring Harbor, NY: Cold Spring Harbor Press

Flechsig E, Shmerling D, Hegyi I, Raeber AJ, Fischer M, Cozzio A, von Mering C, Aguzzi A, Weissmann C (2000) Prion protein devoid of the octapeptide

repeat region restores susceptibility to scrapie in PrP knockout mice. *Neuron* 27: 399–408

Fraser H, Bruce ME, Chree A, McConnell I, Wells GAH (1992) Transmission of bovine spongiform encephalopathy and scrapie to mice. *J Gen Virol* 73: 1891–1897

Gibbings D, Leblanc P, Jay F, Pontier D, Michel F, Schwab Y, Alais S, Lagrange T, Voinnet O (2012) Human prion protein binds Argonaute and promotes accumulation of microRNA effector complexes. *Nat Struct Mol Biol* 19: 517–524, S511

Goldfarb LG, Brown P, McCombie WR, Goldgaber D, Swergold GD, Willis PR, Cerenakova L, Baron H, Gibbs CJ, Gajdusek DC (1991) Transmissible familial Creutzfeldt-Jakob disease associated with five, seven, and eight extra octapeptide coding repeats in the PRNP gene. *Proc Natl Acad Sci USA* 88: 10926–10930

Herms J, Tings T, Gall S, Madlung A, Giese A, Siebert H, Schurmann P, Windl O, Brose N, Kretzschmar H (1999) Evidence of presynaptic location and function of the prion protein. *J Neurosci* 19: 8866–8875

Howells LC, Anderson S, Coldham NG, Sauer MJ (2008) Transmissible spongiform encephalopathy strain-associated diversity of N-terminal proteinase K cleavage sites of PrP(Sc) from scrapie-infected and bovine spongiform encephalopathy-infected mice. *Biomarkers* 13: 393–412

Jackson GS, Murray I, Hosszu LL, Gibbs N, Waltho JP, Clarke AR, Collinge J (2001) Location and properties of metal-binding sites on the human prion protein. *Proc Natl Acad Sci U S A* 98: 8531–8535

Jimenez-Huete A, Lievens PM, Vidal R, Piccardo P, Ghetti B, Tagliavini F, Frangione B, Prelli F (1998) Endogenous proteolytic cleavage of normal and disease-associated isoforms of the human prion protein in neural and non-neural tissues. *Am J Pathol* 153: 1561–1572

Kim C, Haldiman T, Surewicz K, Cohen Y, Chen W, Blevins J, Sy MS, Cohen M, Kong Q, Telling GC et al (2012) Small protease sensitive oligomers of PrPSc in distinct human prions determine conversion rate of PrP(C). *PLoS Pathog* 8: e1002835

Klohn PC, Stoltze L, Flechsig E, Enari M, Weissmann C (2003) A quantitative, highly sensitive cell-based infectivity assay for mouse scrapie prions. *Proc Natl Acad Sci U S A* 100: 11666–11671

Kramer ML, Kratzin HD, Schmidt B, Romer A, Windl O, Liemann S, Hornemann S, Kretzschmar H (2001) Prion protein binds copper within the physiological concentration range. *J Biol Chem* 276: 16711–16719

Kuwahara C, Takeuchi AM, Nishimura T, Haraguchi K, Kubosaki A, Matsumoto Y, Saeki K, Yokoyama T, Itohara S, Onodera T (1999) Prions prevent neuronal cell-line death. *Nature* 400: 225–226

Laffont-Proust I, Faucheux BA, Hassig R, Sazdovitch V, Simon S, Grassi J, Hauw JJ, Moya KL, Haik S (2005) The N-terminal cleavage of cellular prion protein in the human brain. *FEBS Lett* 579: 6333–6337

Langeveld JP, Jacobs JG, Erkens JH, Bossers A, van Zijderveld FG, van Keulen LJ (2006) Rapid and discriminatory diagnosis of scrapie and BSE in retro-pharyngeal lymph nodes of sheep. *BMC Vet Res* 2: 19

Laplanche JL, Hachimi KH, Durieux I, Thuillet P, Defebvre L, Delasnerie-Laupretre N, Peoc'h K, Foncin JF, Destee A (1999) Prominent psychiatric features and early onset in an inherited prion disease with a new insertional mutation in the prion protein gene. *Brain* 122(Pt 12): 2375–2386

Lasmezas CI, Deslys JP, Robain O, Jaegly A, Beringue V, Peyrin JM, Fournier JG, Hauw JJ, Rossier J, Dormont D (1997) Transmission of the BSE agent to mice in the absence of detectable abnormal prion protein. *Science* 275: 402–405

Lauren J, Gimbel DA, Nygaard HB, Gilbert JW, Strittmatter SM (2009) Cellular prion protein mediates impairment of synaptic plasticity by amyloid-beta oligomers. *Nature* 457: 1128–1132

Legname G, Baskakov IV, Nguyen HO, Riesner D, Cohen FE, DeArmond SJ, Prusiner SB (2004) Synthetic mammalian prions. *Science* 305: 673–676

Lewis V, Hill AF, Haigh CL, Klug GM, Masters CL, Lawson VA, Collins SJ (2009) Increased proportions of C1 truncated prion protein protect against cellular M1000 prion infection. *J Neuropathol Exp Neurol* 68: 1125–1135

Mange A, Beranger F, Peoc'h K, Onodera T, Frobert Y, Lehmann S (2004) Alpha- and beta- cleavages of the amino-terminus of the cellular prion protein. *Biol Cell* 96: 125–132

Mays CE, Kim C, Haldiman T, van der Merwe J, Lau A, Yang J, Grams J, Di Bari MA, Nonno R, Telling GC et al (2014) Prion disease tempo determined by host-dependent substrate reduction. *J Clin Invest* 124: 847–858

McDonald AJ, Dibble JP, Evans EG, Millhauser GL (2014) A new paradigm for enzymatic control of alpha-cleavage and beta-cleavage of the prion protein. *J Biol Chem* 289: 803–813

McMahon HE, Mange A, Nishida N, Creminon C, Casanova D, Lehmann S (2001) Cleavage of the amino terminus of the prion protein by reactive oxygen species. *J Biol Chem* 276: 2286–2291

Mead S, Poulter M, Beck J, Webb TE, Campbell TA, Linehan JM, Desbruslais M, Joiner S, Wadsworth JD, King A et al (2006) Inherited prion disease with six octapeptide repeat insertional mutation–molecular analysis of phenotypic heterogeneity. *Brain* 129: 2297–2317

Millhauser GL (2004) Copper binding in the prion protein. *Acc Chem Res* 37: 79–85

Millhauser GL (2007) Copper and the prion protein: methods, structures, function, and disease. *Annu Rev Phys Chem* 58: 299–320

Moore RC, Xiang F, Monaghan J, Han D, Zhang Z, Edstrom L, Anvret M, Prusiner SB (2001) Huntington disease phenocopy is a familial prion disease. *Am J Hum Genet* 69: 1385–1388

Moudjou M, Treguer E, Rezaei H, Sabuncu E, Neuendorf E, Groschup MH, Grosclaude J, Laude H (2004) Glycan-controlled epitopes of prion protein include a major determinant of susceptibility to sheep scrapie. *J Virol* 78: 9270–9276

Mouillet-Richard S, Ermonval M, Chebassier C, Laplanche JL, Lehmann S, Launay JM, Kellermann O (2000) Signal transduction through prion protein. *Science* 289: 1925–1928

Nishida N, Tremblay P, Sugimoto T, Shigematsu K, Shirabe S, Petromilli C, Pilkuhn S, Nakaoke R, Atarashi R, Houtani T et al (1999) Degeneration of Purkinje cells and demyelination in the spinal cord and peripheral nerves of mice lacking the prion protein gene (*Prnp*) is rescued by introduction of a transgene encoded for mouse *Prnp*. *Lab Invest* 79: 689–697

Oesch B, Westaway D, Wälchli M, McKinley MP, Kent SBH, Aebersold R, Barry RA, Tempst P, Teplow DB, Hood LE et al (1985) A cellular gene encodes scrapie PrP 27-30 protein. *Cell* 40: 735–746

Pauly PC, Harris DA (1998) Copper stimulates endocytosis of the Prion Protein. *J Biol Chem* 273: 33107–33110

Prusiner SB (1987) Bioassays of prions. In *Prions - Novel Infectious Pathogens Causing Scrapie and Creutzfeldt-Jakob Disease*, Prusiner SB, McKinley MP (eds), pp 65–81. Orlando: Academic Press

Prusiner SB, Groth DF, Bolton DC, Kent SB, Hood LE (1984) Purification and structural studies of a major scrapie prion protein. *Cell* 38: 127–134

Pushie MJ, Pickering IJ, Martin GR, Tsutsui S, Jirik FR, George GN (2011) Prion protein expression level alters regional copper, iron and zinc content in the mouse brain. *Metallomics* 3: 206–214

Pushie MJ, Vogel HJ (2008) Modeling by assembly and molecular dynamics simulations of the low Cu2+ occupancy form of the mammalian prion protein octarepeat region: gaining insight into Cu2+-mediated beta-cleavage. *Biophys J* 95: 5084–5091

Pushie MJ, Vogel HJ (2009) A potential mechanism for Cu2+ reduction, beta-cleavage, and beta-sheet initiation within the N-terminal domain of the prion protein: insights from density functional theory and molecular dynamics calculations. *J Toxicol Environ Health A* 72: 1040 – 1059

Qin K, Yang DS, Yang Y, Chishti MA, Meng LJ, Kretzschmar HA, Yip CM, Fraser PE, Westaway D (2000) Copper(II)-induced conformational changes and protease resistance in recombinant and cellular PrP. Effect of protein age and deamidation. *J Biol Chem* 275: 19121 – 19131

Qin K, Yang Y, Mastrangelo P, Westaway D (2002) Mapping Cu(II) binding sites in prion proteins by diethyl pyrocarbonate modification and matrix-assisted laser desorption ionization-time of flight (MALDI-TOF) mass spectrometric footprinting. *J Biol Chem* 277: 1981 – 1990

Rangel A, Burgaya F, Gavin R, Soriano E, Aguzzi A, Del Rio JA (2007) Enhanced susceptibility of Prnp-deficient mice to kainate-induced seizures, neuronal apoptosis, and death: role of AMPA/kainate receptors. *J Neurosci Res* 85: 2741 – 2755

Safar JG, Geschwind MD, Deering C, Didorenko S, Sattavat M, Sanchez H, Serban A, Vey M, Baron H, Giles K *et al* (2005) Diagnosis of human prion disease. *Proc Natl Acad Sci U S A* 102: 3501 – 3506

Sandberg MK, Al-Doujaily H, Sharps B, Clarke AR, Collinge J (2011) Prion propagation and toxicity in vivo occur in two distinct mechanistic phases. *Nature* 470: 540 – 542

Sonati T, Reimann RR, Falsig J, Baral PK, O'Connor T, Hornemann S, Yaganoglu S, Li B, Herrmann US, Wieland B *et al* (2013) The toxicity of antiprion antibodies is mediated by the flexible tail of the prion protein. *Nature* 501: 102 – 106

Spevacek AR, Evans EG, Miller JL, Meyer HC, Pelton JG, Millhauser GL (2013) Zinc drives a tertiary fold in the prion protein with familial disease mutation sites at the interface. *Structure* 21: 236 – 246

Spielhaupter C, Schatzl HM (2001) PrPC Directly Interacts with Proteins Involved in Signaling Pathways. *J Biol Chem* 276: 44604 – 44612

Stöckel J, Safar J, Wallace AC, Cohen FE, Prusiner SB (1998) Prion protein selectively binds copper(II) ions. *Biochemistry* 37: 7185 – 7193

Sunyach C, Jen A, Deng J, Fitzgerald KT, Frobert Y, Grassi J, McCaffrey MW, Morris R (2003) The mechanism of internalization of glycosylphosphatidylinositol-anchored prion protein. *EMBO J* 22: 3591 – 3601

Supattapone S, Bosque P, Muramoto T, Wille H, Aagaard C, Peretz D, Nguyen HO, Heinrich C, Torchia M, Safar J *et al* (1999) Prion protein of 106 residues creates an artificial transmission barrier for prion replication in transgenic mice. *Cell* 96: 869 – 878

Szeltner Z, Polgar L (2008) Structure, function and biological relevance of prolyl oligopeptidase. *Curr Protein Pept Sci* 9: 96 – 107

Taraboulos A, Raeber AJ, Borchelt DR, Serban D, Prusiner SB (1992) Synthesis and trafficking of prion proteins in cultured cells. *Mol Biol Cell* 3: 851 – 863

Taubner LM, Bienkiewicz EA, Copie V, Caughey B (2010) Structure of the flexible amino-terminal domain of prion protein bound to a sulfated glycan. *J Mol Biol* 395: 475 – 490

Thakur AK, Srivastava AK, Srinivas V, Chary KV, Rao CM (2011) Copper alters aggregation behavior of prion protein and induces novel interactions between its N- and C-terminal regions. *J Biol Chem* 286: 38533 – 38545

Viles JH, Cohen FE, Prusiner SB, Goodin DB, Wright PE, Dyson HJ (1999) Copper binding to the prion protein:structural implications of four identical cooperative binding sites. *Proc Natl Acad Sci USA* 96: 2042 – 2047

Vincent B, Paitel E, Frobert Y, Lehmann S, Grassi J, Checler F (2000) Phorbol ester-regulated cleavage of normal prion protein in HEK293 human cells and murine neurons. *J Biol Chem* 275: 35612 – 35616

Vincent B, Paitel E, Saftig P, Frobert Y, Hartmann D, De Strooper B, Grassi J, Lopez-Perez E, Checler F (2001) The disintegrins ADAM10 and TACE contribute to the constitutive and phorbol ester-regulated normal cleavage of the cellular prion protein. *J Biol Chem* 276: 37743 – 37746

Walmsley AR, Watt NT, Taylor DR, Perera WS, Hooper NM (2009) alpha-cleavage of the prion protein occurs in a late compartment of the secretory pathway and is independent of lipid rafts. *Mol Cell Neurosci* 40: 242 – 248

Wang F, Wang X, Yuan CG, Ma J (2010) Generating a prion with bacterially expressed recombinant prion protein. *Science* 327: 1132 – 1135

Watt NT, Taylor DR, Gillott A, Thomas DA, Perera WS, Hooper NM (2005) Reactive oxygen species-mediated beta-cleavage of the prion protein in the cellular response to oxidative stress. *J Biol Chem* 280: 35914 – 35921

Weise J, Crome O, Sandau R, Schulz-Schaeffer W, Bahr M, Zerr I (2004) Upregulation of cellular prion protein (PrPc) after focal cerebral ischemia and influence of lesion severity. *Neurosci Lett* 372: 146 – 150

Westaway D, DeArmond SJ, Cayetano-Canlas J, Groth D, Foster D, Prusiner S (1994) Degeneration of skeletal muscle, peripheral nerves, and central nervous system in transgenic mice overexpressing wild-type prion proteins. *Cell* 76: 117 – 129

Westergard L, Turnbaugh JA, Harris DA (2011) A naturally occurring C-terminal fragment of the prion protein (PrP) delays disease and acts as a dominant-negative inhibitor of PrPSc formation. *J Biol Chem* 286: 44234 – 44242

Yadavalli R, Guttmann RP, Seward T, Centers AP, Williamson RA, Telling GC (2004) Calpain-dependent endoproteolytic cleavage of PrPSc modulates scrapie prion propagation. *J Biol Chem* 279: 21948 – 21956